Accepted Manuscript

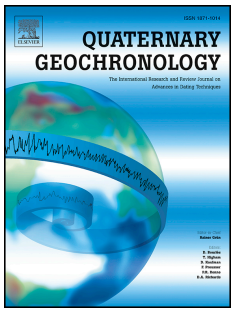

Holocene tephra from the Chukchi-Alaskan margin, Arctic Ocean: Implications for sediment chronostratigraphy and volcanic history

Vera Ponomareva, Leonid Polyak, Maxim Portnyagin, Peter Abbott, Egor Zelenin, Polina Vakhrameeva, Dieter Garbe-Schönberg

PII: S1871-1014(17)30140-1

DOI: 10.1016/j.quageo.2017.11.001

Reference: QUAGEO 878

To appear in: *Quaternary Geochronology*

Received Date: 24 August 2017

Revised Date: 30 October 2017

Accepted Date: 2 November 2017

Please cite this article as: Ponomareva, V., Polyak, L., Portnyagin, M., Abbott, P., Zelenin, E., Vakhrameeva, P., Garbe-Schönberg, D., Holocene tephra from the Chukchi-Alaskan margin, Arctic Ocean: Implications for sediment chronostratigraphy and volcanic history, *Quaternary Geochronology* (2017), doi: 10.1016/j.quageo.2017.11.001.

Holocene tephra from the Chukchi-Alaskan margin, Arctic Ocean: Implications for sediment chronostratigraphy and volcanic history

Vera Ponomareva[a], Leonid Polyak[b], Maxim Portnyagin[c], Peter Abbott[d 1], Egor Zelenin[e], Polina Vakhrameeva[f,g], Dieter Garbe-Schönberg[h]

[a] Institute of Volcanology and Seismology, Piip Boulevard 9, Petropavlovsk-Kamchatsky, 683006, Russia. E-mail: vera.ponomareva1@gmail.com

[b] Byrd Polar and Climate Research Center, Ohio State University, 108 Scott Hall, 109 Carmack Rd., Columbus, OH 43210, USA. E-mail: polyak.1@osu.edu

[c] GEOMAR Helmholtz Center for Ocean Research Kiel, Wischhofstrasse 1-3, 24148 Kiel, Germany. E-mail: mportnyagin@geomar.de

[d] Department of Geography, Swansea University, Singleton Park, Swansea, SA2 8PP, UK. E-mail: abbottp@cardiff.ac.uk

[e] Geological Institute, Pyzhevsky Lane 7, Moscow, 119017, Russia. E-mail: egorzelenin@mail.ru

[f] Institute of Earth Sciences, Heidelberg University, Im Neuenheimer Feld 234, 69120 Heidelberg, Germany. E-mail: polina.vakhrameeva@geow.uni-heidelberg.de

[g] Institute of Earth Sciences, St. Petersburg State University, Universitetskaya Nab. 7-9, 199034, St. Petersburg, Russia

[h] Institute of Geoscience, Christian-Albrechts-University of Kiel, Ludewig-Meyn-Strasse 10, 24118 Kiel, Germany. E-mail: d.garbe-schoenberg@gmx.de

Corresponding author:
Vera Ponomareva,
Institute of Volcanology and Seismology, Piip Boulevard 9, Petropavlovsk-Kamchatsky, 683006, Russia. E-mail: vera.ponomareva1@gmail.com

[1] Now at: Institute of Geological Sciences, University of Bern, Baltzerstrasse 1+3, CH-3012 Bern, Switzerland, and School of Earth and Ocean Sciences, Cardiff University, Park Place, CF10 3AT, Cardiff, UK

Abstract

Developing chronologies for sediments in the Arctic Ocean and its continental margins is an important but challenging task. Tephrochronology is a promising tool for independent age control for Arctic marine sediments and here we present the results of a cryptotephra study of a Holocene sedimentary record from the Chukchi Sea. Volcanic glass shards were identified and quantified in sediment core HLY0501-01 and geochemically characterized with single-shard electron microprobe and laser ablation-inductively coupled plasma-mass spectrometry (LA-ICP-MS). This enabled us to reveal a continuous presence of glass shards with identifiable chemical compositions throughout the core. The major input of glasses into the sediments is geochemically fingerprinted to the ~3.6 ka Aniakchak caldera II eruption (Alaska), which provides an important chronostratigraphic constraint for Holocene marine deposits in the Chukchi-Alaskan region and, potentially, farther away in the western Arctic Ocean. New findings of the Aniakchak II tephra permit a reevaluation of the eruption size and highlight the importance of this tephra as a hemispheric late Holocene marker. Other identified glasses likely originate from the late Pleistocene Dawson and Old Crow tephras while some cannot be correlated to certain eruptions. These are present in most of the analyzed samples, and form a continuous low-concentration background throughout the investigated record. A large proportion of these glasses are likely to have been reworked and brought to the depositional site by currents or other transportation agents, such as sea ice. Overall, our results demonstrate the potential for tephrochronology for improving and developing chronologies for Arctic Ocean marine records, however, at some sites reworking and redistribution of tephra may have a strong impact on the record of primary tephra deposition.

Keywords: Arctic Ocean; Chukchi Sea; marine sediments; cryptotephra; Holocene; volcanic eruption; Aniakchak caldera

1. Introduction

The Chukchi and Beaufort Seas, which extend from the East Siberian to North American continental margin, are experiencing the highest rate of Arctic sea-ice retreat (e.g., Walsh et al., 2016), and thus represent a key area for investigating related processes under both present and past climatic conditions. Several paleoceanographic studies have recently been undertaken on Holocene deposits that accumulated at the Chukchi margin since the last deglaciation and inundation of the shallow shelf (e.g., Keigwin et al., 2006; Darby et al., 2009; Polyak et al., 2016). While at some sites these deposits reach a considerable thickness and provide a fairly high centennial to multidecadal-scale temporal resolution for paleoclimatic proxy reconstructions, this advantage cannot be fully exploited due to problems with developing adequate age constraints. For example, biogenic carbonates suitable for radiocarbon age determination are scarce in these sediments due to widespread dissolution, the total organic matter has a high content of terrestrial material potentially having a wide age range, and the reservoir age in different water masses of the western Arctic is poorly understood (e.g., Faux et al., 2011; Darby et al., 2012; Polyak et al., 2016). Current age models for regional sediment records benefit from the analysis of paleomagnetic secular variations, but the usefulness of this approach varies depending on sedimentation rates and lithology (Barletta et al., 2008; Lisé-Pronovost et al., 2009; Lund et al., 2016).

A promising tool for independent age control of sediments in the Chukchi Sea, and in the Arctic Ocean in general, could be tephrochronology. The Chukchi Sea could be especially promising for tephrochronology as this margin is located close to the volcanically active North Pacific region, which includes the prominent Alaska-Aleutian and Kuril-Kamchatka volcanic arcs. Furthermore, the prevailing direction of winds and currents controls an efficient transportation of suspended sediment and aerosols from this region into and across the Chukchi Sea (e.g., Weingartner et al., 2005; Danielson et al., 2014). As most of the large Holocene tephras from the North Pacific volcanoes have been geochemically fingerprinted and ^{14}C-dated

(e.g., Kyle et al., 2011; Kaufman et al., 2012; Ponomareva et al., 2015, 2017; Davies et al., 2016), their identification in the Arctic sediments will enable accurate correlation to well-dated terrestrial and marine records. Such correlations will provide independent age constraints for Arctic sediment cores and an insight into the marine reservoir effect that impacts ^{14}C dating.

Tephra and cryptotephra occurrences are known from many terrestrial Arctic sites, including Greenland, Svalbard, and northeast Asia (e.g., Abbott and Davies, 2012; Ponomareva et al., 2013a; van den Bogaard et al., 2014; van der Bilt et al., 2017). Visible tephra layers have not been found in Arctic marine sediments, but the presence of cryptotephra in sediments from the Fram Strait connecting the Arctic and Nordic Seas (Zamelczyk et al., 2012), highlights the possibility of finding volcanic deposits in the Arctic Ocean.

Indeed, the first ever studies of tephra in Arctic marine sediments, performed recently at two sites in the Chukchi Sea (Fig. 1), both identified abundant cryptotephra related to the ~3.6 ka Aniakchak II caldera-forming eruption (Ponomareva et al., 2014; Pearce et al., 2017). However, these data also highlighted the complexity of the volcanic signal in the investigated sediments. For example, Pearce et al. (2017) reported a >1.5-m-thick zone of high glass shard concentrations with numerous irregular peaks and minima, rather than a distinct glass shard concentration peak. These results make it difficult to use this cryptotephra as an isochron and pose questions regarding the mechanisms of glass distribution and deposition.

In order to further evaluate the potential of tephrochronology for constraining the age of the western Arctic marine sediments and to investigate tephra transport and deposition patterns, we performed a detailed investigation of cryptotephra in core HLY0501-01 from the sediment accumulation area at the Chukchi-Alaskan margin (preliminary results reported in Ponomareva et al., 2014). The research approach included the quantification of the distribution of tephra in the upper (Holocene) sedimentary unit, determination of the chemical composition of glass shards, especially from tephra occurrence peaks, and matching the fingerprints of identified compositions to known eruptions from the Aleutian and Kuril-Kamchatka volcanic arcs. This

study confirms the presence of tephra with identifiable chemical composition throughout the investigated sediment and provides chronostratigraphic constraints on Holocene marine deposits in the Chukchi-Alaskan region.

2. Study area

The geographic setting of the Chukchi Sea combines its Arctic location with an immediate connection to the Bering Sea via the Bering Strait, and thus defines the important role of this shelf region for water, air-mass, and sediment exchange between the Arctic and North-Pacific realms. Regional hydrographic circulation is dominated by currents originating in the Bering Sea that cross the Chukchi shelf in several branches (Fig. 1; Weingartner et al., 2005). This circulation controls sedimentation largely by removing fine sediment from the shallow areas of the Chukchi and Bering Seas, and depositing it on the northern Chukchi slope, which is characterized by calmer hydrodynamic conditions due to greater water depths and higher sea-ice coverage (e.g., Darby et al., 2009; Polyak et al., 2016). Paleoceanographic studies of sediment cores from the Chukchi margin indicate that this sedimentary regime operated since the stabilization of sea level after the last transgression, ca. 8-9 ka, with some variability primarily attributed to changes in the strength of the Bering Strait Inflow and wind-driven circulation in the Arctic Ocean (Ortiz et al., 2009; Darby et al., 2012; Polyak et al., 2016).

The closest late Quaternary volcanoes to the Chukchi Sea area are monogenetic basaltic lava fields and maars at the Bering Sea margin (Fig. 1; Wood and Kienle, 1990; www.avo.alaska.edu). However, as such fields rarely produce widely dispersed tephra our search for tephra markers in the study area focused on silicic glasses derived from the North Pacific island arc volcanoes located ≥1300 km from the Chukchi margin (Fig. 1). The North Pacific arcs (Kurile-Kamchatka, Alaska-Aleutian and Cascadian) are highly explosive and their glass has been found as cryptotephra over 8000 km from the source (e.g., Pearce et al., 2004; Jensen et al., 2014; Mackay et al., 2016; Bourne et al., 2016; van der Bilt et al., 2017). The closest sites to the

Chukchi margin (~750 km away) where Holocene visible tephra layers have been described, are located on the Seward Peninsula, southwestern Alaska (Fig. 1; Blackford et al., 2014; Davies et al., 2016).

3. Materials and methods

3.1. Core description and sample processing

Sediment core HLY0501-01, composed of a trigger-weight (TC) and a jumbo piston (JPC) cores and supplemented by a nearby multi-core (MC), was collected in 2005 from the northeastern (Alaskan) margin of the Chukchi shelf (Fig. 1; Darby et al., 2005). The coring area is characterized by sediment focusing on the outer shelf and slope, as indicated by subbottom profiling and data from adjacent cores (e.g., Barletta et al., 2008; Darby et al., 2009, 2012; Lisé-Pronovost et al., 2009). The upper sedimentary unit recovered in these cores is composed of fine-grained mud, inferred to represent Holocene marine depositional conditions established after the last deglaciation and concomitant sea-level rise. Grain size data show a rise in coarse fractions (coarser silt and sand) towards the top of the record (Siriwandana, 2014; C.-E. Deschamps, pers. comm.). No visible tephra layers were observed in any of these cores. Core HLY0501-01 was selected for tephra investigation based on the intermediate thickness of the upper unit (slightly over 300 cm), which provides a combination of a sufficiently high temporal resolution with a manageable number of samples for downcore tephra identification. The paleomagnetic stratigraphy of the same core (TC/JPC) has also been investigated, and ^{210}Pb was measured in the MC for evaluating very recent sedimentation rates (Deschamps et al., 2017). No carbonate material for ^{14}C dating has been found in the core, probably due to pervasive dissolution which is common for sediments from the study area (e.g., Darby et al., 2009; Lisé-Pronovost et al., 2009). The TC and JPC were combined into a single section based on the correlation of logged physical properties, such as sediment density, magnetic susceptibility, and color spectral reflectance; akin to TC-JPC correlations for nearby cores (Darby et al., 2009; Ortiz et al., 2009). The HLY0501-

01 correlation indicates a top of JPC to TC offset (estimated 112 cm), which reflects a common JPC overpenetration in soft sediments. Hereafter we are using a composite core depth (in cm) based on the actual TC depth and the offset JPC depth (Fig. 2). We note, however, that the offset may not be consistent downcore because of potentially different stretching or compression of sediment. Based on preliminary paleomagnetic data, the combined record most likely spans the time from ca. 1 to 6 ka (Deschamps et al., 2017). The youngest part of the section was presumably captured by the MC, which collects undisturbed topmost sediments, however, it cannot be accurately correlated to the TC, and is therefore plotted separately from the TC-JPC record (Fig. 2).

Samples were taken in two modes: the upper part of the composite TC/JPC core where high glass concentrations were revealed during reconnaissance research (Ponomareva et al., 2014) was sampled in 2-cm slices while the MC and lower part of JPC were first sampled in 10-cm slabs and then intervals with elevated tephra contents were subsampled in 2-cm slices. Overall, 159 2-cm samples and twenty 10-cm samples were collected along the Holocene sedimentary unit, with a focus on the upper ~200 cm most enriched in tephra. Sample processing was based on methods adopted in marine tephrostratigraphy for extraction of Si-rich glasses (e.g., Abbott et al., 2011, 2013). Freeze-dried samples (0.5 g) were treated consecutively with 10% HCl for four hours and cold 10% NaOH for 1 hour to remove carbonates and to disaggregate clay clumps, respectively, then wet-sieved to obtain the >80 and 25-80 μm size fractions. The latter fraction was then separated using a heavy liquid with a specific gravity of 2.5 g/cm^3. A 2.3 g/cm^3 separation was not required as limited biogenic material was present in the samples following NaOH treatment. It has been suggested that NaOH treatment can affect the geochemical composition of shards (e.g. Blockley et al., 2005), however, experimentation with control samples from Dawson tephra (Alaska) conducted alongside this work found that geochemical analyses were unaffected (Electronic Supplement Table S1 and plots therein). The subfraction lighter than 2.5 g/cm^3 from the 25-80 μm fraction and non-separated >80 μm fraction

were mounted in Canada balsam for glass shard counts. To facilitate the counting of abundant glass shards, samples from the 25-80 µm fraction were spiked with Lycopodium spores and the approach for tephra quantification of Gehrels et al. (2006) was used. Glass concentrations can be found in the Electronic Supplement Tables S2 and S3.

3.2. Volcanic glass analysis

3.2.1. Electron microprobe analysis (EMPA)

Volcanic glass was analyzed in 25 samples from the 25-80-µm fraction using a JEOL JXA 8200 electron microprobe equipped with five wavelength dispersive spectrometers including 3 high-sensitivity ones (2 PETH and TAPH) at GEOMAR (Kiel). The analytical conditions for glasses were a 15 kV accelerating voltage, 6 nA current and 5 µm electron beam size. Analyses were performed in profiles along each slide where every glass shard was analyzed to obtain and quantify a representative set of compositions (Electronic Supplement Tables S4 and S5). Conditions for the electron microprobe analyses and data on reproducibility of reference materials can be found in the Electronic supplement Table S6. More details of the analytical conditions and data reduction can be found in the electronic supplement to Ponomareva et al. (2017).

3.2.2. Laser ablation inductively-coupled plasma mass-spectrometry (LA-ICP-MS) analysis

One of the EMPA-investigated samples was additionally analyzed by single-shard LA-ICP-MS for trace elements in glasses. The analyses were performed using a 193-nm ArF excimer laser system (GeoLas Pro, Coherent) with a large volume ablation cell (ETH Zurich, Switzerland) coupled with a quadrupole-based ICP-MS (Agilent 7500s) at the Institute of Geosciences, Kiel University, Germany). Analyses were performed with 24 µm spots, 5 Hz pulse frequency, and 10 J/cm^2 laser density. Carrier gas was He (~1 l/min) with addition of H2 (14 ml/min), which were mixed with Ar (0.85 l/min) before introduction into spectrometer. Oxide production rate,

estimated as ThO+/Th+, was <0.3%. Analyses were performed in time-resolved mode and included 20 s background measurement followed by 20 s sample ablation and signal measurement. Dwell time was 10 ms for all elements. One isotope per element was measured. The duration of one full mass scan was 0.65 sec. Raw data reduction was performed in Glitter software (Van Achtenbergh et al., 2001) and included subtraction of background from sample signal and selection of time intervals for signal integration, which varied from 3 to 10 s depending on glass shard size and also aimed to avoid occasional contamination of crystal phases. Averaged and ^{43}Ca normalized ion intensities were converted to weight concentrations by using a conventional approach (Longerich et al., 1996), utilizing a sensitivity factor determined on reference material (ATHO-G in this study) and CaO measured by EMPA in the same glass shards or in compositionally similar glasses (rhyodacitic glasses only with average CaO=1.8%) as internal standard. Calibration and drift correction were performed against ATHO-G reference glass and verified using StHs6/80-G and KL2-G glasses (Jochum et al., 2006), which were analyzed as unknown. Concentrations of Si and Ti were analyzed as unknowns and used to screen out analyses contaminated by crystal phases, when their concentrations disagreed with EMPA data by more than 20 rel. %. Single shard LA-ICP-MS analyses, data on reference materials and isotope measured are listed in the Electronic Supplement Table S7.

4. Results

4.1. Glass concentrations

Volcanic glass shards were present in all 179 examined samples, however, significant variation in the concentrations was observed (Fig. 2; Electronic Supplement Tables S2 and S3). The glass counts show a >60 cm thick layer of high glass concentrations in the middle part of the core and a low-concentration background below and above this layer. While the 25-80 μm fraction in the upper and lower parts of the core has a background level of <20000 glass shards per 0.5 g of dry sediment, the middle part between 174 and 110 cm exhibits a sharp increase in glass abundances

with values exceeding 80,000 shards between 154 and 164 cm (Fig. 2a). A similar profile with glass shard concentrations of up to 140 shards within the same depth interval and background values of ≤10 shards is observed in the >80 μm fraction. The overlapping parts of the TC and JPC both show an increase in glass abundances, although the depth of the peaks does not match exactly. The TC glass bulge continues to the bottom of this core, while the JPC peak ends abruptly at 174 cm (composite depth).

Detailed 2-cm samples demonstrate a complex structure of the glass peaks with irregular glass-rich and glass-poor samples (Fig. 2a). In JPC the major peak in glass contents in both 25-80 and >80 μm fractions is observed around ~146-166 cm, with a maximum at 162-166 cm. In the >80 μm fraction this peak is rather narrow with the maximum concentration of glass occurring in three consecutive samples (between 158 and 164 cm) with a short (<10 cm) downward tail and a long (~40 cm) upward tail of lower but above-background glass concentrations (Fig. 2a). In the 25-80 μm fraction, the pattern is quite similar with the exception of one more sharp peak above the background value at ~138 cm. The bottom of the TC record exhibits a more complex pattern with multiple peaks and a major peak in both fractions at 174-176 cm. The pattern of glass shard concentrations in the peak zone suggests that the estimated JPC to TC offset may not be consistent downcore, as the actual position of the tephra peak in the JPC is ~12 cm lower in the composite depth scale (Fig. 2a).

4.2. Glass compositions

4.2.1. Electron microprobe analysis

Microprobe analysis was performed on 25-80 μm glass shards from two 10 cm-samples and twenty three 2 cm-samples (Fig. 2), with a total of 610 individual analyses obtained; an average of 24 analyses per sample (Electronic Supplement Table S4). Analyzed samples cover both glass concentration peaks and the low concentration background signal.

The majority of the HLY0501-01 glass shards form a wide trend in the medium-to high-K field extending from andesite (~56% SiO_2) to rhyolite (~80% SiO_2) (Fig. 3). In addition, there is a small but distinct population of low-to medium-K rhyolitic glasses and a scatter in the high-K rhyolitic field. No low-K glass populations were observed. All the glasses fit into both the Kurile-Kamchatka and Alaskan fields for all analyzed elements (Fig. 3, E Supplement Table S4). Tephras from these volcanic arcs are widely known in the North Pacific-Arctic region (e.g., Elias et al., 1999; Ponomareva et al., 2013a; van den Bogaard et al., 2014; Davies et al., 2016). A comparison to the Kurile-Kamchatka compositions, however, shows that only a few glasses can be matched to known Kamchatka eruptions (see discussion below). In contrast, a comparison to the Alaskan field has allowed us to attribute most glasses to known Alaskan eruptions (Fig. 4).

Most glasses within the medium-to high-K trend are compositionally close to those from the ~3.6 ka Aniakchak II caldera-forming eruption (Alaska) (Fig. 1) (Kaufman et al., 2012; Davies et al., 2016). These glasses form a narrow trend between 55.89% and 71.5% SiO_2, which in some samples splits into separate andesite (~55.9-61% SiO_2) and dacite-rhyolite (~70-71.5% SiO_2) populations. The andesite part of the trend exactly matches that of the reference Aniakchak glasses while the dacite-rhyolite part additionally contains glasses with higher K_2O and FeO and lower Al_2O_3 (Figs. 4 and 5). The Aniakchak II glass composition closely matches that of bulk-rock samples from the Aniakchak-II eruption (Fig. 5): the basaltic andesite-andesite bulk rock trend exactly falls into the glass composition field while bulk rhyolites are slightly lower in SiO_2 contents. Aniakchak II shards are composed of clear glass with very rare crystals (Fig. 6).

The high-Si part of the medium-to-high-K trend combines glasses compositionally close to those from the late Pleistocene Dawson and Old Crow tephras, most likely associated with the Emmons Lake caldera in Alaska (Figs. 1 and 4; Preece et al., 2011; Davies et al., 2016). Tephras of a similar composition have never been reported in Holocene deposits (e.g., Davies et al., 2016). Low-medium-K rhyolitic glasses are close to those from the early Holocene Kurile Lake caldera (South Kamchatka) (KO in Fig. 4). In addition, some HLY0501-01 glasses match those

found by Riehle et al. (1999), however, most of their glasses have CaO contents higher than in HLY0501-01 (Fig. 4c). Some glasses in the high-Si part of the medium-to-high-K trend are close to the White River ash (WRA in Fig. 4a-h; Jensen et al., 2014; Davies et al., 2016), but lack the distinct higher Cl contents of the latter (Fig. 4i).

4.2.2. LA-ICP-MS analysis

Trace elements were analyzed in glass shards from the 154-156 cm interval, where all the EMP analyses showed a distinct Aniakchak II composition, in order to further support identification of this tephra (Fig. 7, Table 1, Electronic Supplement Table S7). Trace elements contents show coherent systematics and correlate well with the major element glass composition. The concentration of most elements, except for Sr, Ti and Eu, increases by ~1.5 times with increasing SiO_2 from ~55% in andesitic glasses to ~70% in rhyodacitic glasses. Sr and Ti exhibit an inverse correlation with SiO_2 and decrease by ~2.5-3 times from andesitic to rhyodacitic compositions. Eu concentration remains nearly constant in all glasses.

The patterns of trace elements normalized to primitive mantle are shown in Fig. 7a, where elements are ordered according to their relative incompatibility with crystal phases in the basaltic system, with the least compatible ("melt-loving") elements placed on the left side of the x-axis and the most compatible ("crystal-loving") on the right. Trace element patterns have a typical shape for intermediate and silicic island-arc magmas. The characteristic island-arc signature is expressed in overall decreasing normalized concentrations from the less to more compatible elements and in a strong selective enrichment in Pb, Rb, Ba, Th, and U, and depletion in Nb, Ta, and Ti relative to REE of similar incompatibility. The patterns of glasses with contrasting SiO_2 are subparallel for the most incompatible elements, indicating their likely origin from the same parental magma. An overall increase in concentrations of trace elements from andesitic to rhyodacitic composition reflects predominant crystallization of trace-element-poor minerals, such as pyroxenes, plagioclase, and Fe-Ti oxides. The anomalous behavior of Ti, Sr, and Eu is

explained by their strong selective partitioning into magnetite, ilmenite (Ti) and plagioclase (Sr, Eu).

As illustrated in Fig. 7b and c, the average trace element compositions of andesitic and rhyodacitic glasses are very similar to the whole rock compositions of crystal-poor andesites and rhyodacites from the 3.6 ka Aniakchak II caldera-forming eruption (e.g., Dreher et al., 2005). The rhyodacitic glasses also have a nearly indistinguishable composition with the clear glass separate from the Aniakchak II pumice, which was used as a reference to identify glass shards from this eruption in the Greenland ice cores (Pearce et al., 2004).

4.3. Distribution of compositionally different glasses in the HLY0501-01 sediments

The down-core distribution of glasses with different compositions is presented in Fig. 2b and c based on the data from Electronic Supplement Tables S4 and S5. The majority of glasses are compositionally close to those from the Aniakchak II eruption. Most of those belong to the rhyolitic population, while andesitic glasses play a subordinate role (Fig. 2b). The appearance of Aniakchak II glasses in HLY0501-01 correlates with a sharp increase in glass concentrations at ~165 cm (JPC). Aniakchak II glasses form a major component of all the samples in the glass concentration zone and are still present in sediments above, up to the top of the core, well after the glass concentrations have returned to the background level. Only two samples above ~165 cm contain exclusively Aniakchak II glasses, while all others have an admixture of compositionally different glasses, from 5 to 52%. Neither 10- nor 2-cm samples taken below the major glass peak contain typical Aniakchak II glasses (except for 3 shards close to the Aniakchak andesite in a sample from 306-308 cm (Fig. 5; Electronic Supplement Table S5).

The proportion of non-Aniakchak II shards is mostly below 20% within the major glass concentration zone and increases up to ~50% above it (Fig. 2b, Electronic Supplement Table S5). The set of compositions of non-Aniakchak II shards remains broadly similar along the core, including (1) glasses close to Aniakchak II but having higher K and Fe, and/or lower Al

contents, (2) Dawson-like, (3) Old Crow-like, and (4) Kurile lake caldera (KO)-like glasses (Figs. 4 and 2c). In addition, two levels of the core have a significant admixture of glasses resembling those from the White River ash (Davies et al., 2016); however, this attribution is tentative and only points at the geochemical type close to the White River ash. Some of the non-Aniakchak-II glasses remain unidentified.

5. Discussion

5.1. Aniakchak II tephra

5.1.1. Aniakchak II caldera-forming eruption

Our research demonstrates that the Holocene deposits at the Chukchi-Alaskan margin contain abundant shards of volcanic glass throughout the investigated section. A major input of glasses into sediments of HLY0501-01 is clearly fingerprinted to the ~3.6 ka Aniakchak caldera II eruption (Alaska), akin to the results presented by Pearce et al. (2017) for a core from the western Chukchi Sea.

The Aniakchak II eruption was globally one of the largest Holocene explosive events: visible tephra was found at the distances of ~1100-1300 km from the source along the western Alaskan coast and in the Bering Sea (Kaufman et al., 2012; Blackford et al., 2014; Derkachev et al., 2015; Graham et al., 2016), and cryptotephra has been reported in northwestern and eastern Canada (Pyne-O"Donnell et al., 2012; Zdanowicz et al., 2014), the Greenland Ice Sheet (Pearce et al., 2004; Coulter et al., 2012) and SE Greenland shelf sediments (Jennings et al., 2014) up to distances of >4500 km from the source (Fig. 1). The eruption produced widespread pumice fall and an extensive ignimbrite sheet (Bacon et al., 2014). Pyroclastic density currents of the eruption entered the Bering Sea and likely generated a tsunami (Waythomas and Neal, 1998). The minimum total volume of bulk material from the Aniakchak II eruption was estimated at >50 km^3, based on considerations of the caldera area, the thickness and distribution of the associated ignimbrite, and comparison with other calderas (Miller and Smith, 1987).

The initial pumice fall had a rhyodacitic bulk composition, while the composition of subsequent ignimbrites varied from rhyodacite to andesite (Bacon et al., 2014). Kaufman et al. (2012) reported both rhyolitic and andesitic glasses in visible tephra layers in Alaska, which suggests that the co-ignimbrite ash could have played some role in the distal tephra fall. Based on the distribution of visible Aniakchak tephra in terrestrial sections from Alaska and in the Bering Sea core (Fig. 1), the ashfall axis was directed northwestwards.

5.1.2. Aniakchak II tephra in core HLY0501-01

The areal distribution of the visible Aniakchak tephra layer, along with the presence of distinct glass concentration peaks in the Chukchi cores, indicates that this peak is a result of a primary tephra fall rather than post-fall redeposition, e.g., by currents, winds, or sea ice. The major peak at ~165 cm in HLY0501-01 (JPC) contains only rhyolitic Aniakchak glasses, while many of the younger intervals also contain andesitic glass shards indicating input from the co-ignimbrite ash (Fig. 2b). The high concentration of the Aniakchak II glasses in both SWERUS-L2-2-PC1 (Pearce et al., 2017) and HLY0501-01 cores (Fig. 1) indicates that this cryptotephra may be found still farther afield and is likely to play a major role in the Holocene stratigraphy of the Arctic Ocean.

We identify the initial rhyolitic Aniakchak II pumice fall, with the newly refined age of 3572±4 cal BP (Pearce et al., 2017), by a sharp increase in the glass contents with entirely Aniakchak II rhyolitic composition in both >80 and 25-80 µm fractions at 164-166 cm in HLY0501-01JPC (Fig. 2a-b). The respective peak at the bottom of the TC appears to occur 12 cm lower in the composite record, which is not surprising, considering inevitable and currently unresolvable inaccuracies of the TC-JPC correlation. The pattern of glass shard concentrations and compositions in the peak zone suggests that the glasses at JPC 164-166 cm and TC 176-178 cm both represent the same initial Aniakchak II tephra fall deposit, which permits further refinement of the relative position of the JPC to TC (Fig. 2a). A less distinct pattern in the TC

tephra distribution below the maximum peak in comparison with the JPC is observed near the core end, where sediment disturbances are probable, so this part of the TC record should be treated with caution.

A rise in coarse fractions towards the top of the record (Siriwandana, 2014; C.-E. Deschamps, pers. comm.) suggests a possible increase in either sea-ice rafting or down-slope sediment transport in the late Holocene. However, no noticeable change occurs around the main tephra peak, indicating that these processes did not have a considerable effect on tephra inputs, and thus confirming the primary fallout signal of the main peak

5.1.3. HLY0501-1 glasses compositionally similar to Aniakchak II

Smaller peaks of Aniakchak II glasses at the intervals around 120 and 140 cm in HLY0501-01JPC (between 142 and 150 cm in the TC) as well as in the upper part of the TC and in the MC may represent either redeposited tephra from the main eruption or additional primary ashfall deposits from younger eruptions. Proximal pyroclastic deposits suggest several post-caldera eruptions with ages ranging from ca. 2.3 ka to 1931 CE (Bacon et al., 2014). At the same time, Kaufman et al. (2012) report two tephras with compositions identical to Aniakchak II and ages of 3.1 and 0.4 ka from lake deposits in southwestern Alaska. As the 3.1 ka eruption is not known in the proximal stratigraphy (Bacon et al., 2014), Kaufman et al. (2012) admitted that this tephra might have been reworked. The same interpretation was suggested for the 0.4 ka tephra as its composition was not found to be identical to the 0.4 ka eruption (Half Cone) from the proximal record. Kaufman et al. (2012), however, mentioned that both ca. 3.1 and 0.4 ka tephras in southwestern Alaska lakes "comprise relatively pure glass, appear to be conformable in the sedimentary sequence and are of indistinguishable age in different lakes" (p. 357), which suggests that they could also be primary ashfall deposits.

The Aniakchak II proximal pyroclastic package as well as the corresponding sequence at the Bering Sea coast, both include several units (Riehle et al., 1999; Bacon et al., 2014). As

revegetation of the pyroclastic sheet and subsequent soil formation on its surface may take hundreds of years (e.g., Grishin and del Moral, 1996), the chronostratigraphy of the proximal record can be hardly resolved on the centennial or higher time scales. This means that the 3.1 ka tephra could have been derived from a separate eruption and form a visible layer in southwest Alaska and a cryptotephra farther north including the Chukchi Sea area. The youngest ~0.4 ka Aniakchak tephra in Kaufman et al. (2012), compositionally identical to the Aniakchak II and ~3.1 ka tephras, might correspond to a small concentration peak in the MC at 36-38 cm, which contains both rhyolitic and andesitic Aniakchak glasses (Fig. 2).

In addition to the major and minor peaks discussed above, background glasses of distinctly Aniakchak II composition are present in the HLY0501-01 sediments starting from ~168 cm and up to the MC top (Fig. 2b). These glasses may result from a continuous transport of tephra particles with sediment load carried by the Alaska Coastal Current from the western Alaskan shores, where Aniakchak II eruptive products crop out along the coastline (Fig. 1; Riehle et al., 1999; Bacon et al., 2014).

5.2. Other glasses

Glasses of non-Aniakchak II compositions are present in most of the analyzed samples forming a continuous background throughout the HLY0501-01 record (Fig. 2b and c). Most of them can be identified as being related to known Alaskan tephras. One glass population is compositionally close to Aniakchak II, but differs from the latter in K and Fe contents (Figs. 4 and 5). This population may have originated from some older Aniakchak eruptions like Black Nose or from other volcanic centers, e.g., Veniaminof eruptive center, where tephras are compositionally close to the Aniakchak (Bacon et al., 2014; Riehle et al., 1999). Other Alaskan glass populations in HLY0501-01 are similar to those from the late Pleistocene Dawson and Old Crow tephras, most likely sourced from the Emmons Lake caldera (Preece et al., 2011; Davies et al., 2016). Because these glasses do not form distinct concentration peaks, but are present at background levels along

451 the entire record, we infer that they were redeposited by sediment transport via the Alaska
452 Coastal Current, as discussed above for the Aniakchak II glasses in the upper part of the core.

453 One of the non-Aniakchak II glass populations compositionally resembles glasses from the
454 ~8.4 ka tephra related to the Kurile Lake caldera-forming eruption in South Kamchatka (coded
455 KO; Ponomareva et al., 2004; Kyle et al., 2011). Both KO airfall deposits and ignimbrites were
456 deposited in the Pacific Ocean and are currently exposed in the coastal cliffs along the Pacific
457 shoreline east of the Kurile Lake (Ponomareva et al., 2004). The presence of these glasses
458 throughout the HLY0501-01 record and the lack of a KO glass concentration peak suggests that
459 these glasses are also products of distal transport from the ash exposures. While depositional
460 conditions at the study site are primarily controlled by the Alaska Coastal Current, other
461 branches of Pacific waters entering the Chukchi Sea may also affect this area, depending on the
462 atmospheric circulation (e.g., Weingartner et al., 2005). The KO-like glass population could
463 alternatively be related to unidentified tephra from the Alaska-Aleutian arc.

464 We did not find any other Kamchatkan tephras, which could be expected in the Chukchi
465 Sea based on their common dispersal axes (Fig. 1). The largest Holocene tephras from
466 Kamchatka, known to make it to eastern Canada, come from the Ksudach volcano: KS_1 and KS_2,
467 dated to ~1.7 and ~7 ka, respectively (Fig. 1; Mackay et al., 2016; Pyne-O'Donnell, pers.comm).
468 These tephras, low-K in composition, do not match any of the HLY0501-01 glasses (Fig. 3; Kyle
469 et al., 2011; Ponomareva et al., 2017). Another large Kamchatkan tephra spread to the north is
470 ~1.5 ka OP from the Opala volcano (Fig. 1; Braitseva et al., 1997; Kyle et al., 2011). OP glasses
471 have high SiO_2 and K_2O contents (~77 and 4%, respectively, Kyle et al., 2011), which do not
472 match any of the glass populations found in HLY0501-01 (Fig. 3). The absence of Kamchatkan
473 tephras, except for glasses probably related to the Kurile Lake caldera, in the middle to late
474 Holocene sediments at the Chukchi-Alaskan margin is not surprising, considering the paucity of
475 prominent Kamchatka eruptions at this time and the prevailing current system. However, we
476 would expect to find them in older Holocene sediments as most of the largest explosive eruptions

in Kamchatka, including KS_2 that reached as far as Svalbard (van der Bilt et al., 2017), occurred prior to ~ 6.5 ka BP (Braitseva et al., 1997). Their prominent absence indirectly corroborates a preliminary age model for HLY0501-01 that implies a hiatus in the early Holocene, potentially caused by sediment erosion by currents or downslope processes (Deschamps et al., 2017). Some of the pre-Holocene Kamchatka eruptions were even more powerful and deposited at least seven visible tephra layers in the El'gygytgyn Lake area, only ~270 km from the Arctic coast (Fig. 1; van den Bogaard et al., 2014).

5.3 Comparison of our trace element data to other measurements for the Aniakchak II tephra

Fig. 7b and c compares compositions of glass shards from this study to proximal whole-rock samples and glasses from visible tephra found in lake sediments from the Ahklun Mountains, southwestern Alaska, which were identified as originating from the Aniakchak caldera II eruption on the basis of their major element systematics (Kaufman et al., 2012). The lake sediment glasses were also analyzed for trace elements by LA-ICP-MS. Unlike glass compositions obtained in this study, rhyodacitic and andesitic glass compositions published by Kaufman et al. (2012) have up to 50% higher concentrations for all trace elements, except for Rb and Cs, as compared to previously published compositions of rocks from the Aniakchak II eruption (Dreher et al., 2015) and also to solution ICP-MS and LA-ICP-MS data generated previously in Aberystwyth (Pearce et al., 2004, 2007) (Fig. 7; Table 1). The difference is particularly large for rhyodacitic glasses. As the ~3.6 ka Aniakchak II tephra is a very prominent Holocene regional marker in Alaska and neighboring areas, and LA-ICP-MS is increasingly being used in tephrochronology, the discrepancy in trace element data is worth evaluating in more detail.

A similar discrepancy between very recent LA-ICP-MS data sets produced in Kiel and Aberystwyth (e.g., Kaufman et al., 2012) was identified for tephra T1 from the El'gygytgyn Lake

(Pearce, 2014; Ponomareva et al., 2013). Pearce (2014) attributed the discrepancy to contamination of analyses in Kiel by crystal phases, namely plagioclase and pyroxene, trapped during laser ablation. However, this does not explain the persistent difference between the two laboratories, especially as the samples measured were represented by pure glass with very rare crystals in both T1 (Pearce, 2014; Ponomareva et al., 2013) and the 3.6 ka Aniakchak II tephras (Kaufman et al., 2012; this study) (Fig. 6). In addition, the spot size applied in the present study was sufficiently small (24 µm), as recommended by Pearce (2014), to avoid entrapment of crystal phases. Such entrapment was effectively recognized by comparing the microprobe and LA-ICP-MS data (see Methods), and the data were excluded from further consideration. Comparisons of this nature are not possible for the Aberystwyth LA-ICP-MS data as concentrations for major elements (e.g. Ti, Ca) are not reported.

The 3.6 ka Aniakchak andesitic and rhyodacitic tephras contain less than 5% of crystals in the glassy matrix (Fig. 6), and therefore whole rocks must have very close compositions with matrix glasses. A remarkably good agreement of our glass compositions with whole rocks as well as with ICP-MS analyses of bulk glass separate (Fig. 7b,c) makes us confident that the trace element data obtained in Kiel are correct and truly characterize the 3.6 ka Aniakchak glasses, in contrast to the poor agreement of Kaufman et al. (2012) glass analyses with the whole rock data. Moreover, data for the 3.6 ka Aniakchak tephra do not report crystal phases able to efficiently fractionate Rb/Th or Cs/Th ratios, which are systematically higher in glass analyses of Kaufman et al. (2012) in comparison with host rocks. Therefore, we argue that the previously published data on Aniakchak glass (Kaufman et al., 2012) lack consistency with electron probe glass data, whole rock compositions and previously published data on the trace element composition of Aniakchak glasses. The difference between the laboratories as well as inconsistency of data generated in Aberystwyth cannot be attributed to contamination by crystal phases, therefore an alternative explanation for the analytical disparity should be sought.

5.4. Application of tephrostratigraphy to Arctic Ocean sediments

Tephra/cryptotephra layers are widely used for dating and synchronizing disparate terrestrial and marine depositional sequences (e.g., Lowe, 2011; Davies, 2015). New terrestrial and marine areas are continuously being explored for their cryptotephra records, which remarkably expands the geography of tephrochronological applications (e.g., China, Sun et al., 2015; Zhao and Hall, 2015; Australia, Coulter et al., 2009; Amazonia, Watson et al., 2015). Our study and the recent research by Pearce et al. (2017) are the first cases of cryptotephra research in the Arctic Ocean, where sedimentary environments are especially challenging for developing reliable age control.

Crytotephra studies of a ~20 ka old sediment core in the Fram Strait connecting the Arctic Ocean with the Nordic seas permitted the identification of three tephras and demonstrated the usefulness of tephrochronology for this area (Zamelczyk et al., 2012). At the same time, glass concentrations in this core, located ~1700 km from the Iceland source volcanoes, were very low, commonly single shards per gram of dry sediment. In contrast, our and Pearce et al.'s (2017) studies in the Western Arctic at distances of ≥1300 km from the closest explosive volcanoes demonstrate high (hundreds or even thousands shards per gram) background glass concentrations reaching greater than 100,000s of shards within the peak of the Aniakchak II glasses (Fig. 2). This pattern attests to the high explosivity of the North Pacific volcanic arcs and to a significant input of volcanic material into marine sediments of the Pacific sector of the Arctic.

The high glass concentrations in the investigated cores are promising for developing a tephrochronological framework for sediments in the Chukchi-Alaskan region. However, as shown by both studies, a large proportion of glasses forming a background signal was likely reworked and brought to the depositional sites by currents or other transportation agents, such as sea ice, and forms a background signal in the records. Large amount of redeposited glasses may obscure the signal of primary, especially minor tephra falls, thus complicating tephrochronological studies.

Volcanic glasses deemed as redeposited in HLY0501-01 have a mostly mixed composition (Fig. 2b and c), which is expected for a long-distance drift averaging over a number of tephra exposures. In contrast, the identification of only rhyolitic Aniakchak II glasses in core SWERUS-L2-2-PC1 from the western Chukchi Sea (Fig. 1; Pearce et al., 2017) is surprising, especially in view of their interpretation that the majority of glasses was transported to the core site from distal primary deposits. In this case one would also expect the sediments to contain andesitic Aniakchak II shards as well as an admixture of other glass populations, as observed in HLY0501-01 except for the major Aniakchak II peak overwhelmed by silicic shards. A possible explanation for the presence of only rhyolitic shards in the western Chukchi Sea is that this area was hit by a rhyolitic fall at the first stage of the Aniakchak II eruption, after which the ashfall axis shifted eastwards ensuring deposition of both rhyolitic and andesitic glasses from the later eruptive stages in HLY0501-01.

Pearce et al. (2017) infer sea ice as the major transporting agent for redeposited sediment, but do not elaborate on the potential sources of redeposition. Their study site in the western Chukchi Sea is primarily affected by the western branch of the Pacific water flowing via the Bering Strait and carrying material from the western side of the Bering Sea (Fig. 1), which limits the possibilities for sediment delivery from the Alaskan coasts. In contrast, the HLY0501-01 site can be affected by both the Alaskan Coastal Current and the eastward-steering continuation of the western branch (Fig. 1). This location is beneficial for sediment delivery from both sides of the northern Bering Sea, however, the Alaskan component clearly predominates, as indicated by HLY0501-01 cryptotephra composition that contains the majority of Alaskan tephras with occasional contributions from the Kurile-Kamchatka region.

We note that Pearce et al. (2017) have geochemically analyzed only four tephra samples, covering a limited time interval of less than 500 years following the Aniakchak II eruption. It is possible that tephra deposited at their site during this time was overwhelmed by the Aniakchak II glass from the primary ashfall and the immediately following redeposition, while older and

younger intervals might contain detectable amounts of other tephras, more in line with the pattern identified in HLY0501-01.

5.5. Aniakchak II tephra volume

The identification of distal tephra brings new information on large eruptions including reappraisal of their volumes and magnitudes. Estimates of eruption magnitudes rely heavily on the knowledge of volumes of air-borne tephra. The existing estimates, however, are very approximate and based mostly on proximal deposits, because their medial and distal counterparts often are poorly mapped and quantified. This is especially true for the Aleutian Islands, where many volcanoes and calderas are located close to the shoreline.

The Aniakchak II tephra is one of the major Holocene tephra markers for the Alaska Peninsula (Davies et al., 2016). Recently obtained data on visible Aniakchak II tephra occurrences in the Bering Sea (Derkachev et al., 2015; Graham et al., 2016) permit significant enlargement of the dispersal area for the Aniakchak II tephra and indicate that it may also be found on the Chukotka Peninsula, the northeastern extremity of Asia (Fig. 1). The wide areal distribution of the Aniakchak II cryptotephra (Fig. 1, inset) in the Chukchi Sea, eastern Canada and Greenland (Pyne-O"Donnell et al., 2012; Pearce et al., 2004; Coulter et al., 2012; Jennings et al., 2014) permits its use as a hemispheric marker for the Holocene deposits.

The new findings of the Aniakchak II tephra layer permit a reassessment of the eruption volume and magnitude. Visible tephra thickness in 14 sites (Kaufman et al., 2012; Blackford et al., 2014; Derkachev et al., 2015; Davies et al., 2016; Graham et al., 2016; Electronic supplement Google Earth file) provide data for isopachs of 1, 5, and 15 cm. Most of the terrestrial tephra findings form two clusters on the Seward Peninsula and in the Ahklun Mountains (SW Alaska) with thickness in adjacent sites varying up to ten times. We use the median thickness of each cluster when constructing isopachs to avoid overestimation of thickness due to tephra redeposition. Furthermore, we exclude the Zagoskin Lake site with a 20-cm thick tephra from

606 the 15 cm isopach as it is possibly redeposited by lake sedimentation. As only a few sites with
607 Aniakchak II tephra have been mapped, the most reliable isopach shape for conservative tephra
608 volume assessment is a convex envelope. The tephra volume is calculated using Weibull fit
609 strategy of thickness-versus-distance semilog plot (Bonadonna and Costa, 2012) and amounts to
610 99 km^3 which is twice larger than previous estimates (Miller and Smith, 1987).

611 There is no common approach to cryptotephra volume assessment as the thickness of
612 deposits is hard to constrain. At the same time, six cryptotephra sites permit to assess the
613 minimal cryptotephra extent. Considering this extent as an isopach of 35 μm (which is the
614 minimal grain size among these sites) and using the same Weibull fitting method (Bonadonna
615 and Costa, 2012) we assess the total tephra volume at 114 km^3 adding another 15 km^3 to the
616 volume estimate based on the visible tephra deposit. The addition of ignimbrite and caldera fill
617 volumes will permit the Aniakchak II eruption rank among the largest Holocene eruptions on
618 Earth, like the Kurile Lake (Kamchatka) (Ponomareva et al., 2004) and Kikai (Japan) (Machida
619 and Arai, 1992) calderas.

620

621 ## 6. Conclusions

622 This study of the Holocene marine sedimentary record at the Chukchi-Alaska margin reveals the
623 continuous presence of volcanic glass shards. A ~50 cm-thick zone of elevated glass
624 concentrations with a distinct peak in the middle part of the record was geochemically
625 fingerprinted to the 3.6 ka Aniakchak II caldera-forming eruption (Alaska), which provides
626 much needed chronological constraints on Holocene marine deposits at the western Arctic
627 continental margins. The high concentration of the Aniakchak II glasses suggests that this tephra
628 can be found still farther afield and serve as a major marker for the late Holocene sediments in
629 the western Arctic Ocean.

630 Non-Aniakchak II glasses have mixed compositions that remain broadly similar along the
631 core and include glasses from known late Pleistocene tephras (Dawson and Old Crow). This

pattern suggests that most of the glasses were redeposited, most likely brought to the eastern Chukchi Sea by the Alaskan Coastal Current. Large amount of redeposited glasses might obscure the signal of primary, especially minor tephra falls, thus complicating tephrochronological applications in the Chukchi Sea.

Single shard trace element on tephra from the major peak in the Artic core further confirms its origin from the Aniakchak II eruption testified by its close match to the proximal glass (Pearce et al., 2004, 2007) and whole-rock compositions (Dreher et al., 2005). Our data confirm previously published results (e.g., Ponomareva et al., 2013b, 2015) that comparison of trace element composition of distal glasses and whole rocks is informative of the tephra provenance, provided the mass-balance of trace elements between matrix glass and mineral phases in whole rocks is taken into account. Aphyric and sparsely-phyric rocks containing no more than a few percent crystals, like those from Aniakchak II eruption, have composition approaching that of matrix glass and are particularly useful in tephrochronology. Even minor amount of mineral phases in whole rocks should be, however, acknowledged as they are able to concentrate certain trace elements and thus cause their coherent depletion in glass relative to the whole rock composition (e.g., Sr and Eu partitions strongly in plagioclase, Zr and Hf in zircon, Ti, Nb, Ta in rutile, REE in apatite).

We note some discrepancies exist between our and previously published LA-ICP-MS data sets on Aniakchak glasses. To facilitate a correct comparison of different sets of data, we point to the necessity of using common reference materials and also reporting data for at least some elements independently analyzed in glasses by electron probe. LA-ICP-MS and electron probe data should be compared to demonstrate their consistency and appropriate analytical setup, which will allow the minimization of potential matrix effects in LA-ICP-MS analyses, arising from unavoidable mismatch between analyzed and reference materials.

Further cryptotephra studies in the North Pacific and Arctic seas will have critical implications for the volcanic history of North Pacific volcanic arcs, especially with the

development of new methods of tephra volume quantification that would incorporate cryptotephra into their models. These efforts will clearly result in a reappraisal of the power of past explosive eruptions and their temporal patterns, which will bring a better understanding of future volcanic events and their impact on humankind.

Acknowledgements

This research was supported by the Russian Science Foundation grant #16-17-10035. The Otto Schmidt Laboratory funded by the German Federal Ministry for Education and Research (BMBF) partly supported VP visits to GEOMAR for tephra analyses. LP's contribution was supported by the US National Science Foundation award ARC-0612493. PMA was financially supported by the European Research Council (TRACE project) under the European Union's Seventh Framework Programme (FP7/2007-2013)/ERC grant agreement no. [259253]. Authors thank Siwan Davies (Swansea University) for advice and support and Gareth James (Swansea University) for laboratory support. We acknowledge the GEOMAR Helmholtz Center funding for the electron microprobe analyses. We thank Mario Thöner and Ulrike Westernströer for their assistance with electron probe and LA-ICP-MS analyses. We are grateful to Stefan Wastegård and an anonymous reviewer for their comments and suggestions.

References

Abbott, P.M., Davies, S.M., Austin, W.E., Pearce, N.J., Hibbert, F.D., 2011. Identification of cryptotephra horizons in a North East Atlantic marine record spanning Marine Isotope Stages 4 and 5a (~60,000–82,000 a b2k), Quat. Int., 246, pp. 177-189, doi: 10.1016/j.quaint.2011.07.033.

Abbott, P.M., Davies, S.M., 2012. Volcanism and the Greenland ice-cores: the tephra record, Earth-Sci. Rev., 115, pp. 173-191, doi: 10.1016/j.earscirev.2012.09.001.

683 Abbott, P.M., Austin, W.E.N., Davies, S.M., Pearce, N.J.G., Hibbert, F.D., 2013.
684 Cryptotephrochronology of a North East Atlantic marine sequence over Termination II, the
685 Eemian and the last interglacial-glacial transition, J. Quat. Sci., 28, 501-514, doi:
686 10.1002/jqs.2641.
687 Barletta, F., St-Onge, G., Channell, J.E.T., Rochon, A., 2010. Dating of Holocene western
688 Canadian Arctic sediments by matching paleomagnetic secular variation to a geomagnetic
689 field model, Quat. Sci. Rev., 29, pp. 2315–2324, doi: 10.1016/j.quascirev.2010.05.035.
690 Bindeman, I.N., Fournelle, J.H., Valley, J.W., 2001. Low-δ 18 O tephra from a compositionally
691 zoned magma body: Fisher Caldera, Unimak Island, Aleutians, J. Volcanol. Geotherm. Res.,
692 111, 35-53, doi: 10.1016/S0377-0273(01)00219-0.
693 Blackford, J. J., Payne, R. J., Heggen, M. P., de la Riva Caballero, A., van der Plicht, J., 2014.
694 Age and impacts of the caldera forming Aniakchak II eruption in western Alaska, Quat. Res.,
695 82, pp. 85–95, doi:10.1016/j.yqres.2014.04.013.
696 Blockley, S.P.E., Pyne-O'Donnell, S.D.F., Lowe, J.J., Matthews, I.P., Stone, A., Pollard, A.M.,
697 Turney, C.S.M., Molyneux, E.G., 2005. A new and less destructive laboratory procedure for
698 the physical separation of distal glass tephra shards from sediments, Quat. Sci. Rev., 24, pp.
699 1952-1960, doi: 10.1016/j.quascirev.2004.12.008.
700 Bourne, A.J., Abbott, P.M., Albert, P.G., Cook, E., Pearce, N.J., Ponomareva, V., Svensson, A.,
701 Davies, S.M., 2016. Underestimated risks of recurrent long-range ash dispersal from northern
702 Pacific Arc volcanoes, Sci. Rep., 6, doi: 10.1038/srep29837.
703 Braitseva, O. A., Ponomareva, V. V., Sulerzhitsky, L. D., Melekestsev, I. V., Bailey, J., 1997.
704 Holocene key-marker tephra layers in Kamchatka, Russia, Quat. Res., 47, pp. 125-139,
705 doi:10.1006/qres.1996.1876.
706 Carson, E.C., Fournelle, J.H., Miller, T.P., Mickelson, D.M., 2002. Holocene tephrochronology
707 of the Cold Bay area, southwest Alaska Peninsula, Quat. Sci. Rev., 21, pp. 2213-2228, doi:
708 10.1016/S0277-3791(02)00023-9.

709 Coulter, S.E., Turney, C.S., Kershaw, P., Rule, S., 2009. The characterization and significance of
710 a MIS 5a distal tephra on mainland Australia, Quat. Sci. Rev., 28, pp. 1825-1830, doi:
711 10.1016/j.quascirev.2009.04.018.
712 Coulter, S.E., Pilcher, J.R., Plunkett, G., Baillie, M., Hall, V.A., Steffensen, J.P., et al., 2012.
713 Holocene tephras highlight complexity of volcanic signals in Greenland ice cores, J.
714 Geophys. Res., Atmospheres, 117, D21303, doi:10.1029/2012JD017698.
715 Danielson, S.L., Weingartner, T.J., Hedstrom, K.S., Aargaard, K., Woodgate, R., Curchister, E.,
716 Stabeno, P.J., 2014. Coupled wind-forced controls of the Bering-Chukchi shelf circulation
717 and the Bering Strait throughflow: Ekman transport, continental shelf waves, and variations
718 of the Pacific-Arctic sea surface height gradient, Progress in Oceanography, 125, pp. 40–61,
719 doi:10.1016/j.pocean.2014.04.006.
720 Darby, D., Jakobsson, M., Polyak, L., 2005. Icebreaker expedition collects key Arctic seafloor
721 and ice data, Eos, 86, pp. 549–556, doi:10.1029/2005EO520001.
722 Darby, D.A., Ortiz, J. Polyak, L., Lund, S., Jakobsson, M., Woodgate, R.A., 2009. The role of
723 currents and sea ice in both slowly deposited central Arctic and rapidly deposited Chukchi-
724 Alaskan margin sediments, Global Planet. Change 68, pp. 58–72,
725 doi:10.1016/j.gloplacha.2009.02.007.
726 Darby, D.A., Ortiz, J.D., Grosch, C.E., Lund, S.P., 2012 1,500-year cycle in the Arctic
727 Oscillation identified in Holocene Arctic sea-ice drift, Nature Geoscience, 5, pp. 897□900,
728 doi:10.1038/ngeo1629.
729 Davies, L. J., Jensen, B. J., Froese, D. G., Wallace, K. L., 2016. Late Pleistocene and Holocene
730 tephrostratigraphy of interior Alaska and Yukon: Key beds and chronologies over the past
731 30,000 years, Quat. Sci. Rev., 146, pp. 28-53, doi: 10.1016/j.quascirev.2016.05.026.
732 Davies, S.M., 2015. Cryptotephras: the revolution in correlation and precision dating, J. Quat.
733 Sci., 30, pp. 114-130, doi: 10.1002/jqs.2766.

734 Derkachev A.N., Portnyagin M.V., Ponomareva V.V., Gorbarenko S.A., Malakhov M.I.,
735 Nikolaeva N.A., Nuernberg D., Shi Xuefa, Liu Yanguang, 2015. Marker tephra layers of
736 large explosive eruptions from volcanoes of Aleutian Islands and Alaska in Quaternary
737 deposits of the Bering Sea, Materials of the XXI International Conference (School) on
738 Marine Geology, 16-20 November 2015, Moscow, v. 1, pp. 107-111, 2015 [In Russian].
739 http://geoschool.ocean.ru/index.php/arkhiv-konferentsii/category/10-materialy-xxi-shkoly-
740 po-morskoj-geologii-2015.html
741 Deschamps, C.-E., St-Onge, G., Montero-Serrano, J.-C., and Polyak, L., 2017, accepted.
742 Chronostratigraphy and spatial distribution of magnetic sediments in the Chukchi and
743 Beaufort seas since the last deglaciation. Boreas.
744 Dreher, S.T., Eichelberger, J.C., and Larsen, J.F., 2005. The petrology and geochemistry of the
745 Aniakchak caldera-forming ignimbrite, Aleutian Arc, Alaska, J. Petrol., 46, pp. 1747-1768,
746 doi:10.1093/petrology/egi032.
747 Elias, S.A., Hamilton, T.D., Edwards, M.E., Begét, J.E., Krumhardt, A.P., Lavoie, C., 1999. Late
748 Pleistocene environments of the western Noatak basin, northwestern Alaska, Geol. Soc.
749 Amer. Bull., 111, pp. 769-789, doi: 10.1130/0016-
750 7606(1999)111<0769:LPEOTW>2.3.CO;2.
751 Faux J.F., Belicka, L.L., Harvey, H.R., 2011 Organic sources and carbon sequestration in
752 Holocene shelf sediments from the western Arctic Ocean, Cont. Shelf Res., 31, pp. 1169–
753 1179, doi:10.1016/j.csr.2011.04.001.
754 Gehrels, M.J., Lowe, D.J., Hazell, Z.J., Newnham, R.M., 2006. A continuous 5300-yr Holocene
755 cryptotephrostratigraphic record from northern New Zealand and implications for
756 tephrochronology and volcanic hazard assessment, The Holocene, 16, pp. 173-187,
757 doi:10.1191/0959683606hl918rp.
758 Gill, J.B., 1981. Orogenic andesites and plate tectonics. Springer, Berlin, 390 p.

759 Graham, R.W., Belmecheri, S., Choy, K., Culleton, B.J., Davies, L.J., Froese, D., Heintzman,
760 P.D., Hritz, C., Kapp, J.D., Newsom, L.A., Rawcliffe, R., 2016. Timing and causes of mid-
761 Holocene mammoth extinction on St. Paul Island, Alaska, P. Nat. Acad. Sci. USA, 113, pp.
762 9310-9314, doi: 10.1073/pnas.1604903113.
763 Grishin, S.Y., del Moral, R., 1996. Dynamics of forests after catastrophic eruptions of
764 Kamchatka's volcanoes, Biodiversity and the dynamics of ecosystems, DIWPA series, 1, pp.
765 133-146.
766 Jennings, A., Thordarson, T., Zalzal, K., Stoner, J., Hayward, C., Geirsdóttir, Á., Miller, G.,
767 2014. Holocene tephra from Iceland and Alaska in SE Greenland shelf sediments, Geol. Soc.,
768 London, Spec. Publ., 398, pp. 157-193, doi: 10.1144/SP398.6.
769 Jensen B.J., Pyne-O'Donnell, S., Plunkett, G., Froese, D.G., et al., 2014. Transatlantic
770 distribution of the Alaskan White River Ash, Geology, 42, pp. 875-878,
771 doi:10.1130/G35945.1.
772 Jochum, K. P., Stoll, B., Herwig, K., Willbold, M., Hofmann, A.W., Amini, M., Aarburg, S.,
773 Abouchami, W., Hellebrand, E., Mocek, B., Raczek, I., 2006. MPI-DING reference glasses
774 for in situ microanalysis: new reference values for element concentrations and isotope ratios,
775 Geochem. Geophy. Geosy., 7, Q02008, doi:10.1029/2005GC001060.
776 Kaufman, D.S., Jensen, B.J.L., Reyes, A.V., et al., 2012. Late Quaternary tephrostratigraphy,
777 Ahklun Mountains, SW Alaska, J. Quat. Sci. 27, pp. 344–359, doi:10.1002/jqs.1552.
778 Keigwin, L.D., Donnelly, J.P., Cook. M.S., Driscoll, N.W., Brigham-Grette, J., 2006. Rapid sea-
779 level rise and Holocene climate in the Chukchi Sea, Geology, 34, pp. 861–864,
780 doi:10.1130/G22712.1.
781 Lisé-Pronovost, A., St-Onge, G., Brachfeld, S., Barletta, F., Darby, D., 2009. Paleomagnetic
782 constraints on the Holocene stratigraphy of the Arctic Alaskan margin, Global Planet.
783 Change, 68, pp. 85-99, doi:10.1016/j.gloplacha.2009.03.015.

784 Longerich, H.P., Jackson, S.E., Günther, D., 1996. Laser ablation inductively coupled plasma
785 mass spectrometric transient signal data acquisition and analyte concentration calculation, J.
786 Anal. Atom. Spectrom., 11, pp. 899-904, doi: 10.1039/Ja9961100899.
787 Lowe, D.J., 2011. Tephrochronology and its application: A review, Quat. Geochronol., 6, pp.
788 107-153, doi: 10.1016/j.quageo.2010.08.003.
789 Lund, S., Keigwin, L.D., Darby, D.A., 2016. Character of Holocene paleomagnetic secular
790 variation in the tangent cylinder: Evidence from the Chukchi Sea, Phys. Earth Planet. In.,
791 256, pp. 49–58, doi:10.1016/j.pepi.2016.03.005.
792 Mackay, H., Hughes, P.D., Jensen, B.J., Langdon, P.G., Pyne-O'Donnell, S.D., Plunkett, G.,
793 Froese, D.G., Coulter, S., Gardner, J.E., 2016. A mid to late Holocene cryptotephra
794 framework from eastern North America, Quat. Sci. Rev., 132, pp. 101-113,
795 doi:10.1016/j.quascirev.2015.11.011.
796 Machida, H., Arai, F., 1992. Atlas of Tephra in and Around Japan. Tokyo Univ. Press, Tokyo.
797 Miller, T.P., Smith, R.L., 1987. Late Quaternary caldera forming eruptions in the eastern
798 Aleutian arc, Alaska, Geology, 1, pp. 434–438, doi:10.1130/0091-
799 7613(1987)15<434:LQCEIT>2.0.CO;2.
800 Ortiz, J.D., Polyak, L., Grebmeier, J.M., Darby, D.A., Eberl, D.D., 2009. Provenance of
801 Holocene clay minerals on the Chukchi Shelf, Alaska, based on combined diffuse spectral
802 reflectance and quantitative X-Ray Diffraction, Global Planet. Change, 68, pp. 73–84,
803 doi:10.1016/j.gloplacha.2009.03.020.
804 Pearce, C., Varhelyi, A., Wastegård, S., Muschitiello, F., Barrientos, N., O'Regan, M., Cronin,
805 T.M., Gemery, L., Semiletov, I., Backman, J., Jakobsson, M., 2017. The 3.6 ka Aniakchak
806 tephra in the Arctic Ocean: a constraint on the Holocene radiocarbon reservoir age in the
807 Chukchi Sea, Clim. Past, 13, pp. 303-316, doi:10.5194/cp-2016-112.

Pearce, N.J., 2014. Towards a protocol for the trace element analysis of glass from rhyolitic shards in tephra deposits by laser ablation ICP-MS. J.Quat. Sci., 29, pp. 627-640, doi: 10.1144/SP398.1.

Pearce, N.J., Westgate, J.A., Preece, S.J., Eastwood, W.J., Perkins, W.T., 2004. Identification of Aniakchak (Alaska) tephra in Greenland ice core challenges the 1645 BC date for Minoan eruption of Santorini, Geochem. Geophy. Geosy., 5(3), doi: 10.1029/2003GC000672.

Pearce, N.J., Denton, J.S., Perkins, W.T., Westgate, J.A., Alloway, B.V., 2007. Correlation and characterisation of individual glass shards from tephra deposits using trace element laser ablation ICP-MS analyses: current status and future potential. J. Quat. Sci., 22, pp. 721-736, doi: 10.1002/jqs.1092.

Pendea, I.F., Ponomareva, V., Bourgeois, J., Zubrow, E.B., Portnyagin, M., Ponkratova, I., Harmsen, H., Korosec, G., 2017. Late Glacial to Holocene paleoenvironmental change on the northwestern Pacific seaboard, Kamchatka Peninsula (Russia), Quat. Sci. Rev., 157, pp. 14-28, doi: 10.1016/j.quascirev.2016.11.035.

Polyak, L., Belt, S.T., Cabedo-Sanz, P., Yamamoto, M., Park, Y.-H., 2016. Holocene sea-ice conditions and circulation at the Chukchi-Alaskan margin, Arctic Ocean, inferred from biomarker proxies, The Holocene, 26, pp. 1810–1821, doi:10.1177/0959683616645939.

Ponomareva, V., Portnyagin, M., Derkachev, A., Juschus, O., Garbe-Schönberg, D., Nürnberg D., 2013a. Identification of a widespread Kamchatkan tephra: a middle Pleistocene tie-point between Arctic and Pacific paleoclimatic records, Geophys. Res. Lett., 40/14, pp. 3538–3543; doi: 10.1002/grl.50645.

Ponomareva, V., Portnyagin, M., Derkachev, A., Pendea, I.F., Bourgeois, J., Reimer, P.J., Garbe-Schönberg, D., Krasheninnikov, S., Nürnberg, D., 2013b. Early Holocene M~6 explosive eruption from Plosky volcanic massif (Kamchatka) and its tephra as a link between terrestrial and marine paleoenvironmental records, Int. J. Earth Sci. 102, pp. 1673-1699, doi: 10.1007/s00531-013-0898-0.

834 Ponomareva, V., Polyak, L., Portnyagin, M., Abbott, P. M., Davies, S. M., 2014. A Holocene
835 cryptotephra record from the Chukchi margin: the first tephro-stratigraphic study in the
836 Arctic Ocean, Proceedings of the 2nd Past Gateways international conference and workshop,
837 Trieste, 2014, pp. 69-70.
838 Ponomareva, V., Portnyagin, M., Davies, S., 2015. Tephra without borders: Far-reaching clues
839 into past explosive eruptions, Frontiers in Earth Science/Volcanology, 3, 83,
840 doi:10.3389/feart.2015.00083.
841 Ponomareva, V., Portnyagin, M., Pendea, F., Zelenin, E., Bourgeois, J., Pinegina, T., Kozhurin,
842 A., 2017. A full Holocene tephrochronology for the Kamchatsky Peninsula region:
843 applications from Kamchatka to North America, Quat. Sci. Rev., 168, pp. 101-122, doi:
844 10.1016/j.quascirev.2017.04.031.
845 Preece, S.J., Pearce N.J.G., Westgate J.A., Froese D.G., Jensen B.J.L., Perkins W.T., 2011. Old
846 Crow tephra across eastern Beringia: a single cataclysmic eruption at the close of Marine
847 Isotope Stage 6, Quat. Sci. Rev., 30, pp. 2069–2090, doi:10.1016/j.quascirev.2010.04.020.
848 Riehle, J. R., Meyer, C. E., Miyaoka, R. T., 1999. Data on Holocene tephra (volcanic ash)
849 deposits in the Alaska Peninsula and lower Cook Inlet region of the Aleutian volcanic arc,
850 Alaska, U.S. Geological Survey Open-File Report OF 99-0135, 5 p.
851 Siriwardana, C.H.E.R., 2014. Characterization of paleoclimate and marine processes associated
852 with Holocene sedimentation on the Chikchi margin, Arctic Ocean. PhD Thesis, Kent State
853 University, 171 p.
854 Sun, C., You, H., He, H., Zhang, L., Gao, J., Guo, W., et al., 2015. New evidence for the
855 presence of Changbaishan Millennium eruption ash in the Longgang volcanic field,
856 Northeast China, Gondwana Res, doi: 10.1016/j.gr.2015.01.013.
857 Van Achterbergh, E., Ryan, C.G., Jackson, S.E., Griffin,W.L., 2001. Data reduction software for
858 LA-ICP-MS: appendix. In: Sylvester, P.J. (Ed.), Laser Ablation-ICP-Mass Spectrometry in

the Earth Sciences: Principles and Applications, Mineralog. Assoc.Canada (MAC) Short Course Series, Ottawa, Ontario, Canada, 29, pp. 239–243.

van den Bogaard, C., Jensen, B.J.L., Pearce, N.J.G., Froese, D.G., Portnyagin, M.V., Ponomareva, V.V., Wennrich, V., 2014. Volcanic ash layers in Lake El'gygytgyn: eight new regionally significant chronostratigraphic markers for western Beringia, Clim. Past, 10, pp. 1041-1062, doi:10.5194/cp-10-1041-2014.

van der Bilt, W.G., Lane, C.S., Bakke, J., 2017. Ultra-distal Kamchatkan ash on Arctic Svalbard: Towards hemispheric cryptotephra correlation, Quat. Sci. Rev., 164, pp. 230-235, doi:10.1016/j.quascirev.2017.04.007.

Walsh, J. E., F. Fetterer, J. S. Stewart, Chapman, W. L., 2017. A database for depicting Arctic sea ice variations back to 1850, Geogr. Rev., 107, pp. 89-107, doi:10.1111/j.1931-0846.2016.12195.x.

Watson, E.J., Swindles, G.T., Savov, I.P., Bacon, K.L., 2015. First discovery of Holocene cryptotephra in Amazonia, Sci. Rep., 5, 15579, doi: 10.1038/srep15579.

Waythomas, C.F., Neal, C.A., 1998. Tsunami generation by pyroclastic flow during the 3500-year BP caldera-forming eruption of Aniakchak Volcano, Alaska, Bull. Volcanol., 60, pp. 110-124, doi:10.1007/s004450050.

Weingartner, T., Aagaard, K., Woodgate, R., Danielson, S., Sasaki, Y., Cavalieri, D., 2005. Circulation on the north central Chukchi Sea shelf, Deep-Sea Res. II, 52, pp. 3150–3174, doi:10.1016/j.dsr2.2005.10.015.

Wood Ch.A. and Kienle J. (Eds) 1990. Volcanoes of North America: United States and Canada. Cambridge University Press.

Zamelczyk K, Rasmussen TL, Husum K, et al., 2012. Paleoceanographic changes and calcium carbonate dissolution in the central Fram Strait during the last 20 ka, Quaternary Res., 78, pp. 405–416, doi:10.1016/j.yqres.2012.07.006.

Zdanowicz, C., Fisher, D., Bourgeois, J., Demuth, M., Zheng, J., Mayewski, P., Kreutz, K., Osterberg, E., Yalcin, K., Wake, C., Steig, E. J., Froese, D., Goto-Azuma, K., 2014. Ice cores from the St. Elias Mountains, Yukon, Canada: Their significance for climate, atmospheric composition and volcanism in the North Pacific region, Arctic, 67, pp. 35–57, doi:10.14430/arctic4352.

Zhao, H., Hall, V.A., 2015. Assessing the potential for cryptotephra studies in Northeastern China, The Holocene, 25, pp. 772-783, doi: 10.1177/0959683615569320.

Table 1.

Average trace element compositions of glasses from sample HLY0501-JPC_42-44 (154-156 cm composite depth) and reference compositions of Aniakchak II rocks and glasses

Figure captions

Fig. 1. Map showing locations of the Chukchi Sea sediment cores HLY0501-01 (this paper) and SWERUS-L2-2-PC1 (Pearce et al., 2017), sites with visible Aniakchak II tephra, and axes or dispersal areas of major ash falls in the area. Aniakchak II sites according to Kaufman et al. (2012), Blackford et al. (2014), Derkachev et al. (2015), Davies et al. (2016), and Graham et al. (2016). Dispersal areas and ashfall axes of tephras mentioned in the text - Kamchatka: KO - Kurile Lake caldera, ~8.4 ka (Ponomareva et al., 2004); Rauchua - supposedly Karymsky volcanic center, ~177 ka (Ponomareva et al., 2013); OP - Barany Amphitheater, Opala volcano, ~1.5 ka; KS_1 and KS_2 - Ksudach calderas, ~1.7 and 6.8 ka, respectively (Braitseva et al., 1997; Kyle et al., 2011); Alaska: Old Crow and Dawson tephras supposedly from the Emmons Lake calderas, ~124 and 30 ka, respectively (Preece et al., 2011; Davies et al., 2016). Aniakchak II dispersal area is based on visible tephra sites. Blue and green arrows show major Pacific water currents in the Chukchi Sea: Alaskan Coastal Current (green) and other branches carrying Bering Sea waters (blue); dashed arrows show pathways of the western branch continuation (from Weingartner et al., 2005;

http://psc.apl.washington.edu/HLD/Chukchi/Chukchi.html). Inset shows Aniakchak II (red circles), and KS_1 and KS_2 (yellow circles) cryptotephra sites (Pearce et al., 2004; Pyne-O'Donnell et al., 2012, pers. comm; Coulter et al., 2012; Zdanowicz et al., 2014; Mackay et al., 2016, van der Bilt et al., 2017).

Fig. 2. Concentration and composition of volcanic glass found in core HLY0501-01 (TC – trigger core, JPC – jumbo piston core, MC – multi-corer).

a - Amount of glass shards per 0.5 g of dry sediment in >80 and 25-80 µm fractions. Gray outline shows glass concentration in 10-cm samples; red filled curve and red outline - in 2-cm samples in the upper and lower part of the TC, respectively; turquoise filled curve - in 2-cm JPC samples. Analyzed samples are marked with dark blue dots (2-cm samples) or bars (10-cm samples). **b and c** - Distribution of compositionally different glasses in the 25-80 µm fraction: b - Proportion of the Aniakchak II and other shards (rhyolitic and andesitic Aniakchak II shards are shown separately with red and pink colors, respectively; other glasses are shown in dark blue). Amount of glass shards per 0.5 g of dry sediment for the upper part of the TC and JPC is shown with gray shade. c - Proportion of compositionally different shards within the non-Aniakchak-II glasses. Glasses compositionally close to the Aniakchak II ones are shown in orange and pink; those close to Dawson ones - in green, Old Crow - in purple, Kurile Lake (KO) - in turquoise, White River ash (WRA?) - in yellow, non-identified glasses - in dark blue.

Fig. 3. Compositions of HLY0501-01 volcanic glasses compared to those from the Kurile-Kamchatka and Alaska tephras. Kurile-Kamchatka compositional field based on Ponomareva et al., 2013a,b; 2015; 2017; Portnyagin and Ponomareva, unpublished data. Alaska field based on Riehle et al., 1999; Bindeman et al., 2001; Preece et al., 2011; Kaufman et al., 2012; Bacon et al., 2014; Carson et al., 2002; Davies et al., 2016. All analyses used here and

in the following bi-plots are normalized on unhydrous basis. Low-, medium- and high-K fields are shown after Gill (1981).

Fig. 4. Compositions of HLY0501-01 volcanic glasses compared to known large Alaska and Kamchatka tephras. Aniakchak II (~3.6 ka) tephra from the Aniakchak II caldera (Kaufman et al., 2012; Bacon et al., 2014; Davies et al., 2016); late Pleistocene Dawson and Old Crow tephras supposedly from the Emmons Lake caldera (Alaska) (Preece et al., 2011; Davies et al., 2016); KO - tephra from the Kurile Lake caldera (Kamchatka); WRA - White River ash from the Bona-Churchill volcanic massif (Jensen et al., 2014; Davies et al., 2016). Alaska high-K medium-to low-K glasses based on Riehle et al., 1999, Bindeman et al., 2001; and Carson et al., 1999. **i)** shows all the range of Cl contents in the WRA tephras while other plots show only glasses with Cl<0.32 - the limit for Cl in the HLY0501-01 glasses.

Fig. 5. Geochemical diagrams showing details of glass compositions falling into the Aniakchak II trend. Aniakchak II trend is illustrated by the rhyolitic glass population (JPC sample from the major glass concentration peak at 162-164 cm composite depth) and andesite-rhyolite trend observed in the younger JPC samples (150-152 and 120-122 cm composite depth, respectively). Pre-Aniakchak II glasses are from JPC samples from 260-262, 240-242, and 234-244 cm composite depth). Reference compositions of the Aniakchak II glasses are from Kaufman et al. (2012), bulk rock - from Bacon et al. (2014). Pre-Aniakchak II glasses have dacitic to high-Si rhyolitic compositions characterized by higher K and Fe, and lower Al contents.

Fig. 6. Microscopic images of ca. 3.6 ka Aniakchak II glass shards from core HLY0501-01 (depth 158-160 cm, sample HLY0501-JPC_46-48).

962 **Fig. 7.** Trace element composition of the Aniakchak II glass shards. **a**. Major groups of glasses
963 identified on the basis of their major element composition: andesitic (A) - SiO_2=57-54%,
964 dacitic (D) - SiO_2=60-65%, rhyodacitic (RD) - SiO_2>68%; **b**. Comparison of average
965 composition of the Aniakchak II andesitic glasses from core HLY0501-01 with the
966 Aniakchak II andesite pumice (Dreher et a., 2005) and andesitic glasses from the Alaska lake
967 sediments (Kaufman et al., 2012); c. Comparison of average composition of Aniakchak II
968 rhyodacitic glasses from core HLY0501-01 with the Aniakchak II rhyodacite pumice (Dreher
969 et a., 2005), clear glass separate from rhyodacite pumice (Pearce et al., 2004), rhyodacitic
970 glasses (Pearce et al., 2007), and rhyodacitic glasses from the Alaska lake sediments
971 (Kaufman et al., 2012).
972

973

Table 1. Average trace element compositions of glasses from sample HLY0501-JPC_42-44 (154-156 cm composite depth) and reference compositions of Aniakchak II rocks and glasses

	Andesitic glasses this study*		**Average Aniakchak II whole rock andesite Ref. 1****		**Dacitic glasses this study***		**Rhyodacitic glasses this study***		**Average Aniakchak II whole rock rhyodacite Ref. 1****		**Aniakchak II rhyodacitic glass Ref.2****	**Aniakchak II rhyodacitic glass Ref.3***
Element	Mean (n=3)	2s	Mean (n=2)	2s	Mean (n=3)	2s	Mean (n=12)	2s	Mean (n=3)	2s		
Li	17.9	(1.6)			22.6	(8.4)	27.7	(5.2)				
Ti	8761	(282)	8100	(848)	5701	(2640)	2896	(268)	3180	(208)		
Rb	37.3	(7.4)	33.3	(8.2)	53.1	(16.2)	68.9	(10.0)	65.6	(2.2)	66.5	72.3
Sr	504	(78)	456	(42)	312	(114)	195	(28)	225	(6)	199	235
Y	37.0	(2.6)	36.0	(4.2)	45.5	(4.4)	49.4	(8.6)	49.2	(1.6)	46.3	43.9
Zr	148	(13)	137	(28)	246	(28)	295	(54)	239	(6)	267	233
Nb	9.32	(1.0)	8.75	(2.04)	10.9	(6.4)	16.6	(2.8)	15.0	(0.4)	15.5	13.3
Cs	1.93	(0.50)	1.53	(0.42)	2.68	(1.30)	3.48	(0.84)	2.96	(0.1)	3.11	
Ba	531	(16)	511	(62)	745	(200)	880	(170)	843	(30)	861	727
La	19.0	(0.8)	18.8	(3.2)	23.4	(3.4)	27.3	(6.0)	26.8	(0.4)	26.4	30.3
Ce	39.8	(4.2)	38.9	(3.2)	49.9	(4.4)	57.1	(11.4)	54.0	(1.0)	57.4	56.5
Pr	5.74	(0.38)	5.10	(0.72)	6.92	(0.68)	7.39	(1.42)	6.82	(0.22)	6.96	8.07
Nd	26.9	(3.9)	23.6	(2.6)	30.6	(2.0)	32.5	(5.8)	30.1	(0.4)	30.6	31.1
Sm	6.18	(0.60)	6.46	(0.74)	7.29	(1.18)	7.61	(1.34	7.87	(0.08)	7.66	8.17
Eu	2.27	(0.48)	2.03	(0.16)	2.02	(0.14)	2.09	(0.42)	2.07	(0.04)	1.71	2.12
Gd	6.96	(1.43)	6.59	(0.62)	7.49	(0.84)	8.30	(1.46)	7.99	(0.16)	6.54	8.88
Tb	1.04	(0.04)	1.10	(0.10)	1.39	(0.34)	1.29	(0.24)	1.34	(0.02)	1.27	1.43
Dy	6.27	(1.32)	6.60	(0.42)	7.73	(1.48)	8.27	(1.54)	8.28	(0.24)	7.74	8.72
Ho	1.28	(0.18)	1.36	(0.16)	1.67	(0.12)	1.72	(0.32)	1.74	(0.04)	1.82	1.84
Er	3.87	(0.46)	3.65	(0.32)	4.68	(0.46)	5.25	(1.32)	4.90	(0.10)	4.84	5.01
Tm	0.58	(0.14)	0.53	(0.08)	0.80	(0.06)	0.80	(0.26)	0.74	(0.04)	0.73	0.77
Yb	3.62	(1.14)	3.26	(0.28)	5.12	(1.02)	5.45	(1.86)	4.67	(0.04)	4.78	5.45
Lu	0.60	(0.22)	0.53	(0.08)	0.73	(0.18)	0.76	(0.12)	0.77	(0.02)	0.74	0.84

Hf	4.06	(0.68)	3.71	(0.68)	6.87	(1.06)	7.43	(1.34)	6.89	(0.10)	7.12	5.84
Ta	0.67	(0.14)	0.61	(0.16)	0.77	(0.46)	1.01	(0.26)	1.01	(0.04)	1.03	0.71
Pb	7.32	(1.70)	6.14	(1.32)	10.8	(4.4)	12.2	(2.4)	11.0	(0.6)		
Th	3.52	(0.48)	3.11	(0.02)	5.50	(1.32)	6.85	(1.48)	5.48	(0.18)	6.13	6.55
U	1.47	(0.44)	1.44	(0.56)	2.34	(1.34)	3.11	(0.68)	2.63	(0.10)	2.84	2.64

Note. * LA-ICP-MS; **solution ICP-MS. References: 1 – Dreher et al. (2015), 2- Pearce et al. (2004), 3 – Pearce at al. (2007). 2s – two standard deviations.

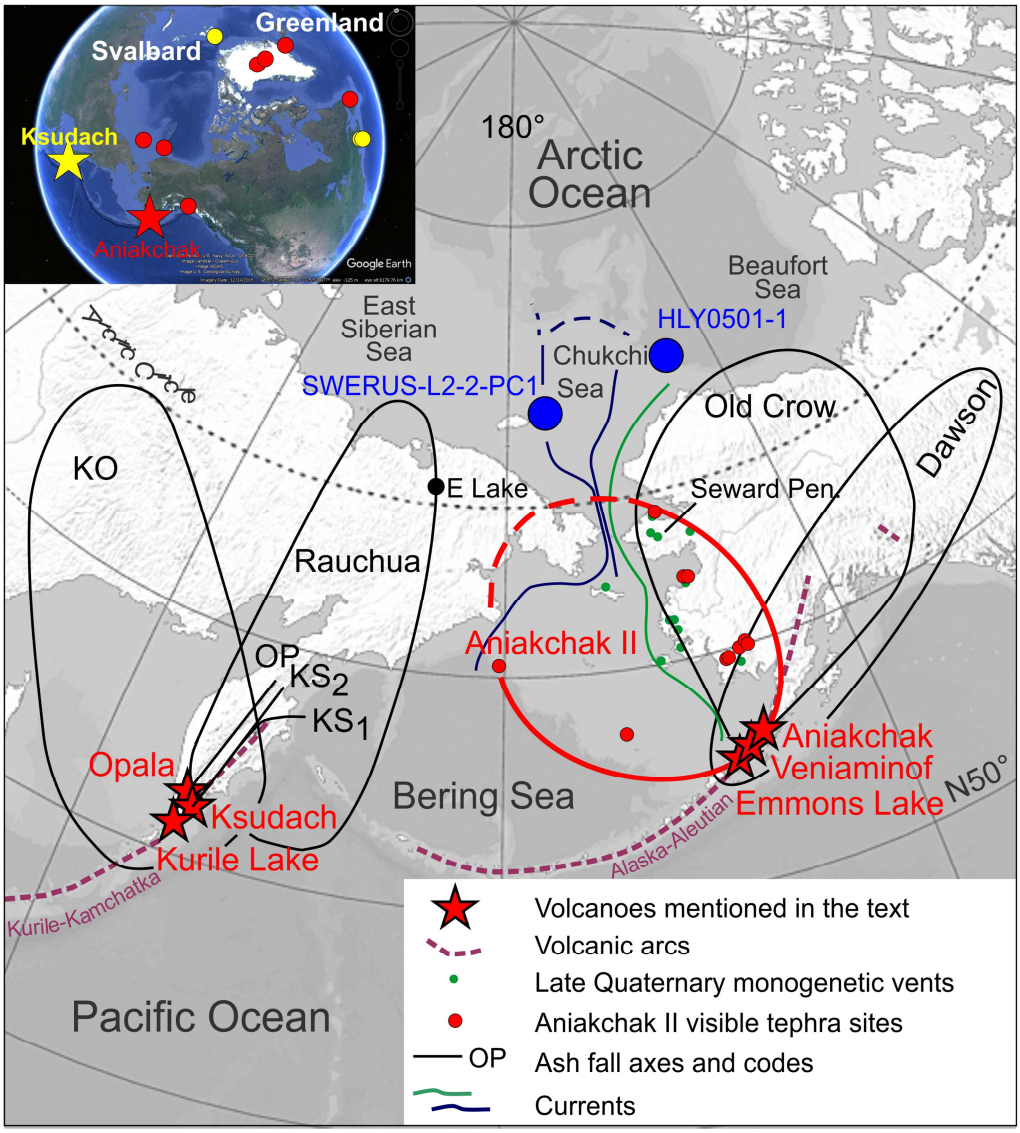
Greenland
Svalbard
Ksudach
Aniakchak
Google Earth
180°
Arctic Ocean
Beaufort Sea
East Siberian Sea
HLY0501-1
Chukchi Sea
SWERUS-L2-2-PC1
Old Crow
Dawson
Arctic Circle
KO
E Lake
Seward Pen.
Rauchua
Aniakchak II
OP
KS2
KS1
Opala
Ksudach
Kurile Lake
Bering Sea
Aniakchak
Veniaminof
Emmons Lake
N50°
Alaska-Aleutian
Kurile-Kamchatka
Pacific Ocean
Volcanoes mentioned in the text
Volcanic arcs
Late Quaternary monogenetic vents
Aniakchak II visible tephra sites
OP
Ash fall axes and codes
Currents

Fig. 1

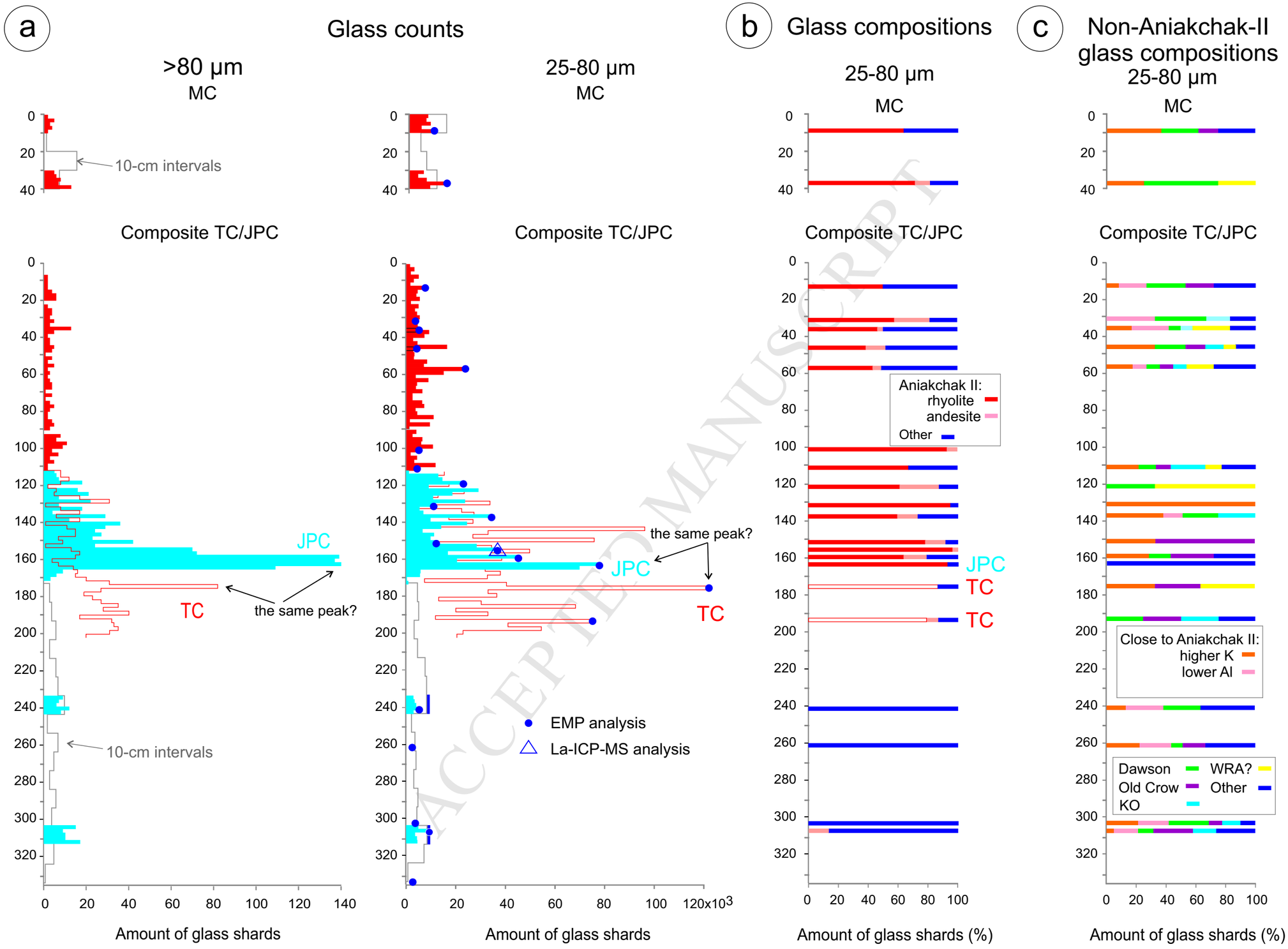

Fig. 2

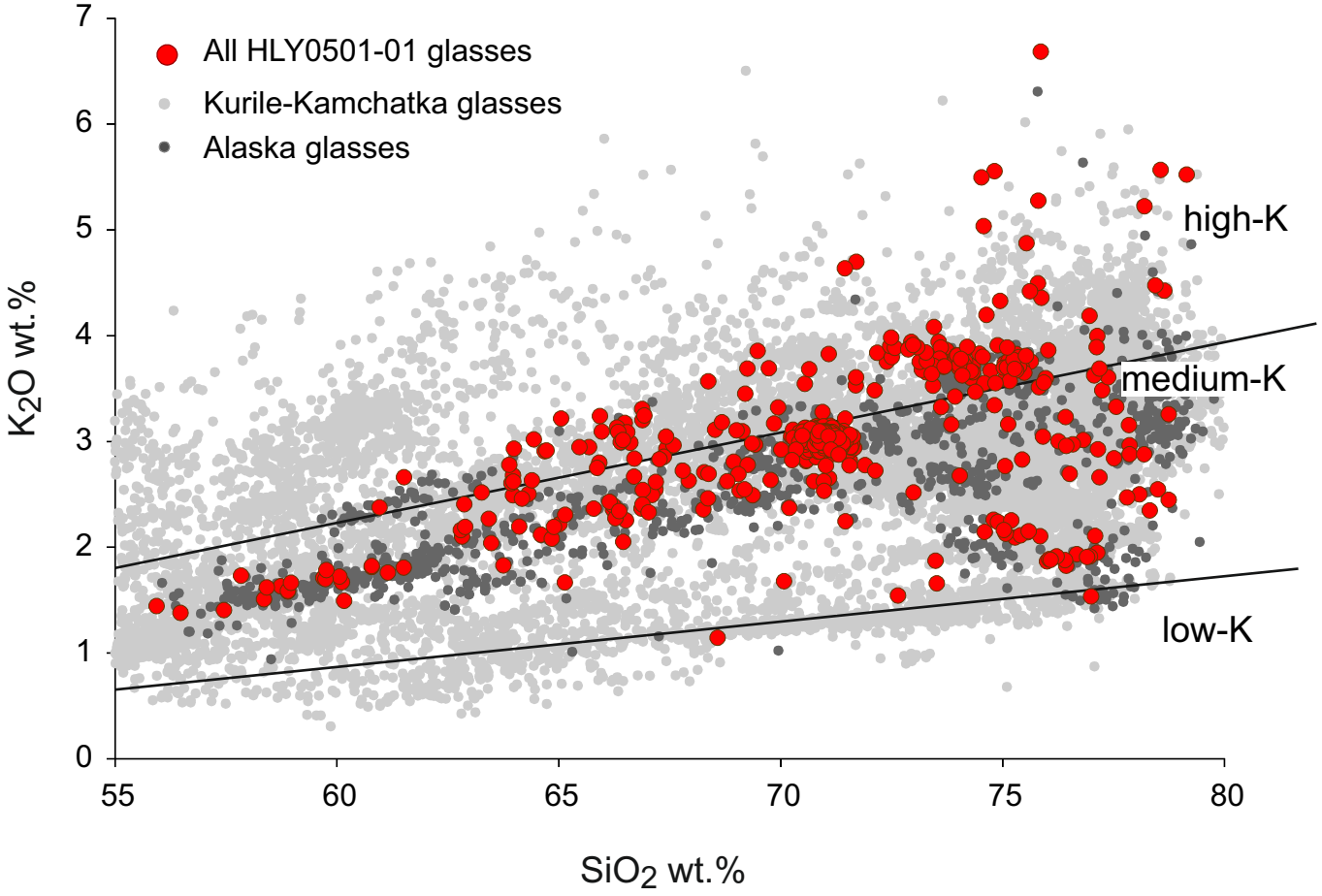
All HLY0501-01 glasses
Kurile-Kamchatka glasses
Alaska glasses
high-K
medium-K
low-K
K_2O wt.%
SiO_2 wt.%
0
1
2
3
4
5
6
7
55
60
65
70
75
80

Fig. 3

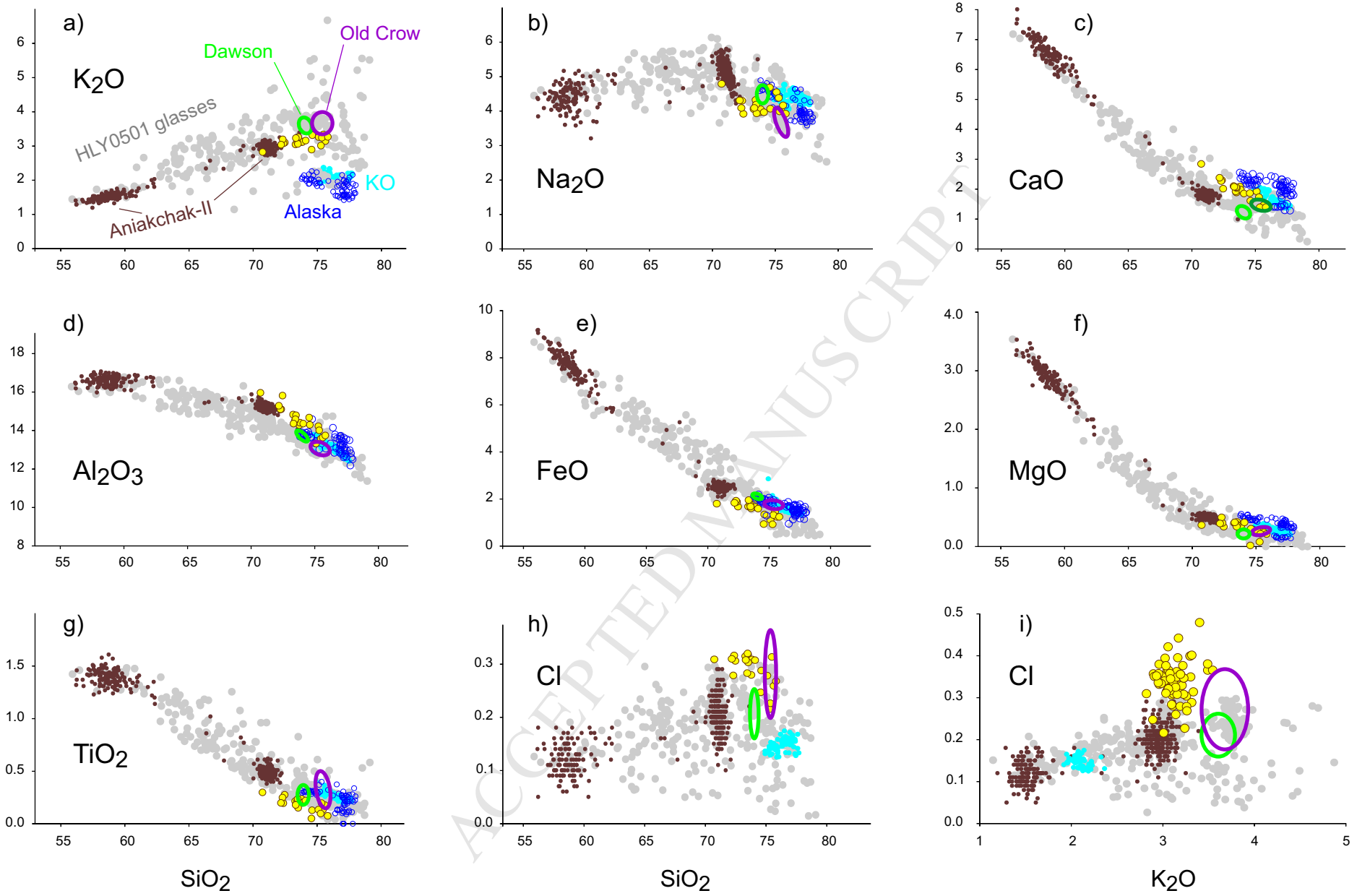

Fig. 4

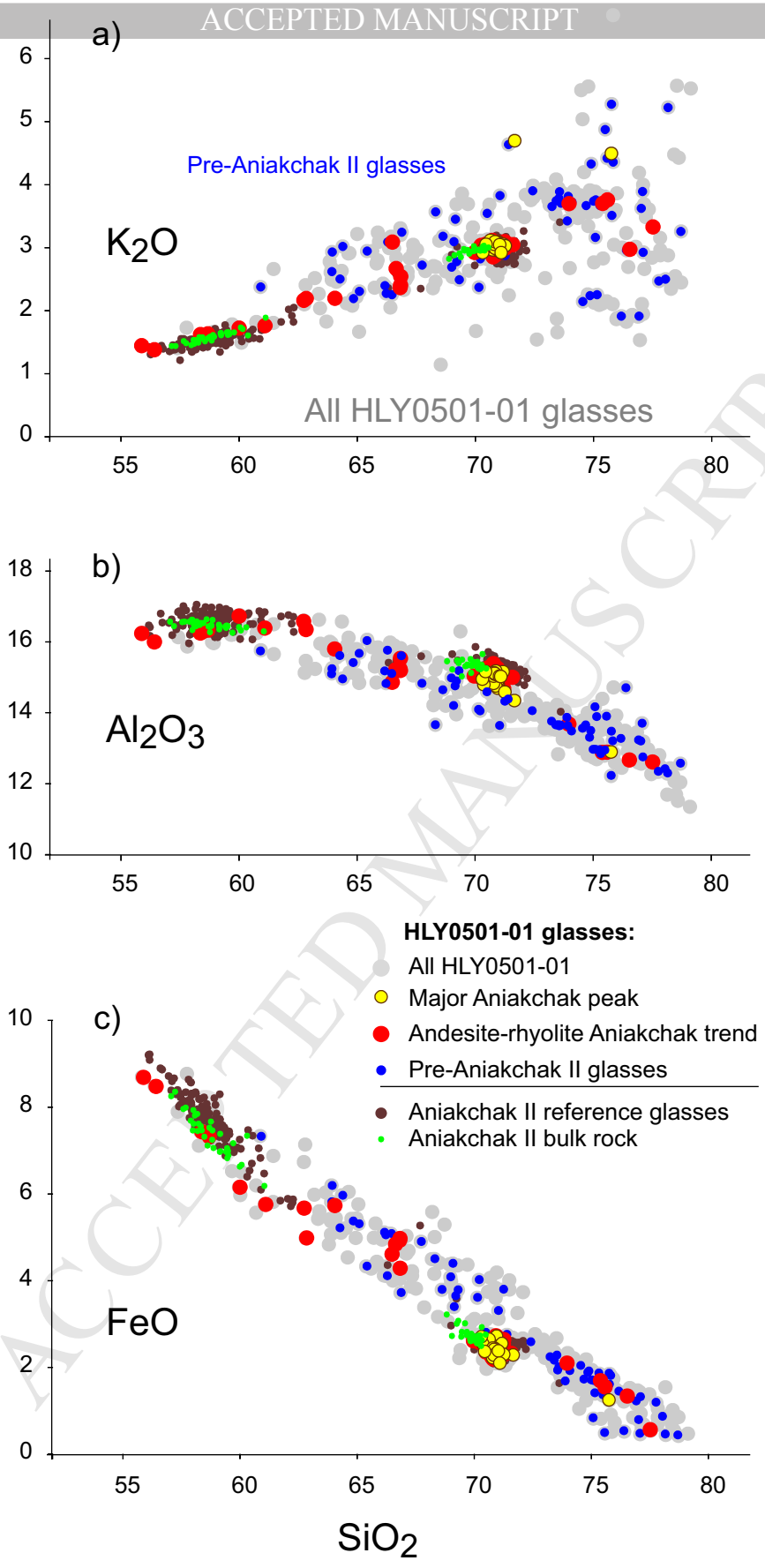

Fig. 5

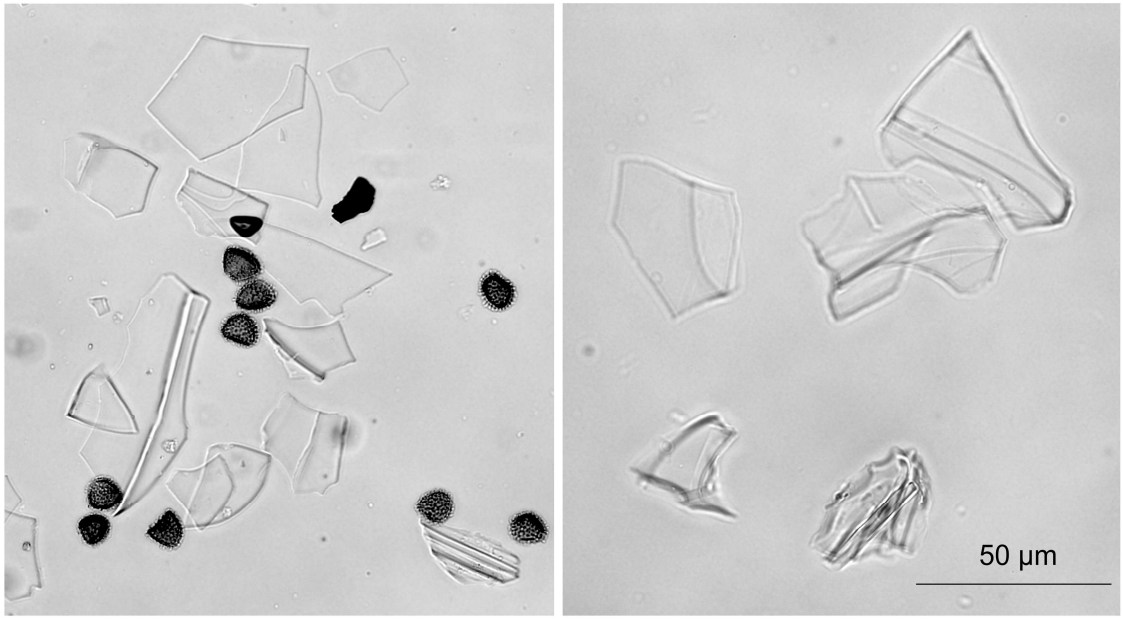

Fig. 6

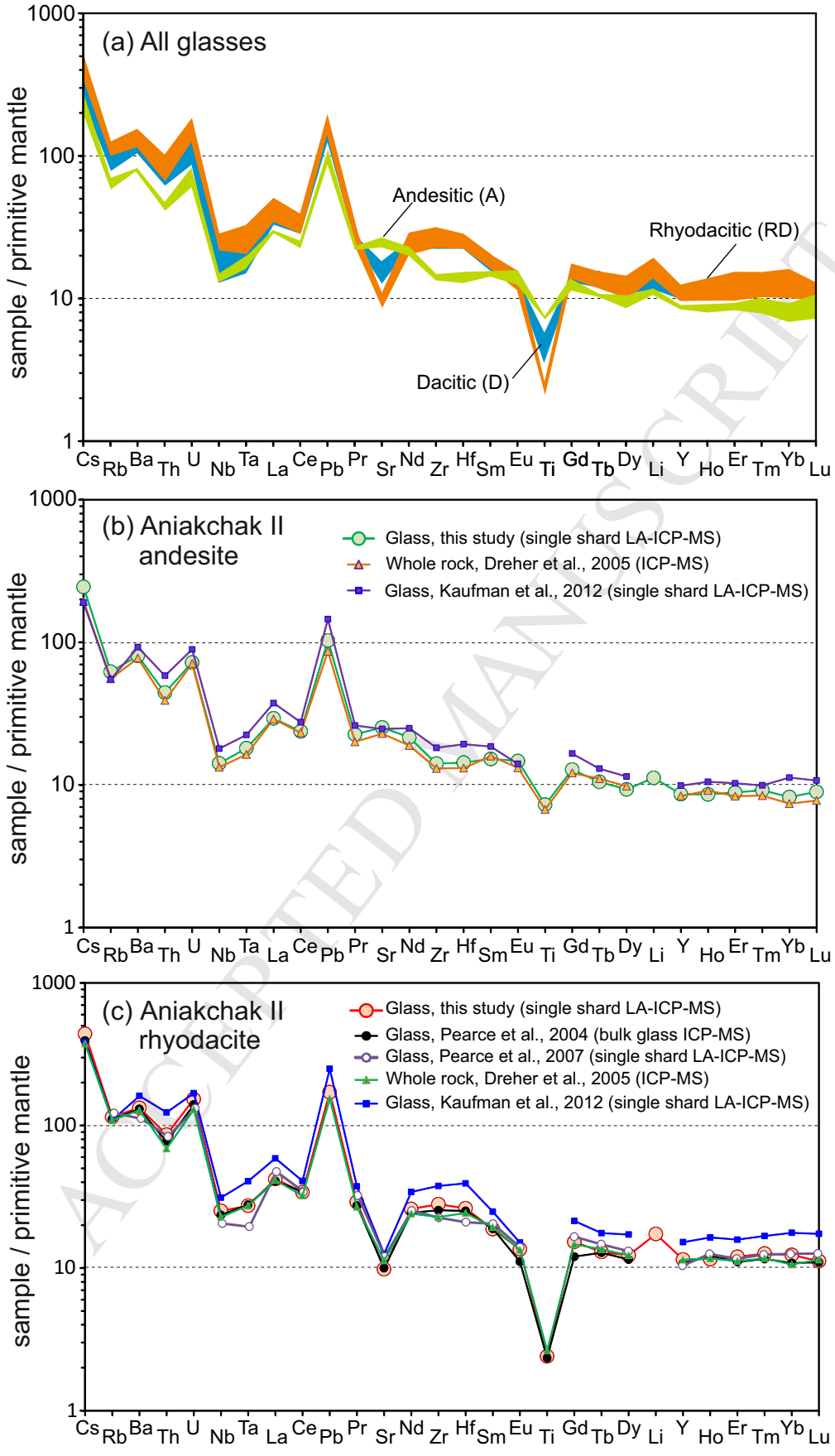
(a) All glasses
Andesitic (A)
Rhyodacitic (RD)
Dacitic (D)
(b) Aniakchak II andesite
Glass, this study (single shard LA-ICP-MS)
Whole rock, Dreher et al., 2005 (ICP-MS)
Glass, Kaufman et al., 2012 (single shard LA-ICP-MS)
(c) Aniakchak II rhyodacite
Glass, this study (single shard LA-ICP-MS)
Glass, Pearce et al., 2004 (bulk glass ICP-MS)
Glass, Pearce et al., 2007 (single shard LA-ICP-MS)
Whole rock, Dreher et al., 2005 (ICP-MS)
Glass, Kaufman et al., 2012 (single shard LA-ICP-MS)
sample / primitive mantle
1000
100
10
1
Cs Rb Ba Th U Nb Ta La Ce Pb Pr Sr Nd Zr Hf Sm Eu Ti Gd Tb Dy Li Y Ho Er Tm Yb Lu

Fig. 7

Ponomareva et al. "Holocene tephra from the Chukchi-Alaskan margin, Arctic Ocean: Implications for sediment chronostratigraphy and volcanic history"

Highlights:

- Cryptotephra study of a Holocene sedimentary record from the Chukchi Sea
- Major tephra concentration peak fingerprinted to the ~3.6 ka Aniakchak eruption
- New electron microprobe and LA-ICP-MS glass data applicable for the Western Arctic
- Re-evaluation of the Aniakchak tephra volume
- Redeposited tephra shards map pathways of sediment transport